Revision 2

Field and model constraints on silicic melt segregation by compaction/hindered settling: the role of water and its effect on latent heat release

Cin-Ty A. Lee[1*], Douglas M. Morton[2], Michael J. Farner[1], Pranabendu Moitra[1]

[1]Department of Earth Science, MS-126, Rice University, 6100 Main St., Houston, TX 77005, USA
[2]Department of Earth Sciences and United States Geological Survey, 900 University Ave., University of California, Riverside, CA 92521, USA

Words in abstract: 265
Words in text: 6503
10 Figures, 1 Table, 7 Supplementary Tables

*corresponding author, ctlee@rice.edu

To investigate how large volumes of silicic melts segregate to form granitic plutons, we conducted a case study of a zoned pluton, in which SiO_2 increases from intermediate (69 wt. %) to highly silicic compositions (74 wt. %) toward the contact with metasedimentary wallrock. All other major, minor and trace elements vary systematically with SiO_2 and indicate that outward increasing SiO_2 is due to a decrease in mafic elements and minerals. Whole-rock oxygen isotopes and elemental variation diagrams do not support mixing with wallrock as an explanation for the Si-rich boundary layer. Instead, mafic enclaves are common in the pluton, but decrease in abundance in the outer 25 m of the pluton, suggesting a mechanical origin for the Si-rich boundary layer. These observations, combined with geochemical modeling, indicate that the silica-rich, enclave-poor boundary layer formed by hindered settling or compaction of a crystal-rich (crystal fractions > 60 %) magmatic mush. Segregation of melts at high crystal fraction is known to be a slow process. However, petrography and Zr-based thermometry indicate that the residual Si-rich liquids were water-saturated. Water decreases melt viscosity, which helps expulsion, but equally importantly, water also delays much of the latent heat release to late in the thermal and crystallization history of a cooling magma. We show that the higher the water content, the longer the time interval over which a magma chamber resides at the stage when water-saturated, high silica liquids form, allowing sufficient time for exfiltration of silicic liquids before the magma body freezes.

Introduction

The ubiquity of highly silicic igneous rocks, such as granites, at Earth's surface makes our planet unique in the solar system (Campbell and Taylor, 1983; Taylor and McLennan, 1985). Of interest are how magmas with SiO_2 contents greater than 70 wt. % are formed. Volumetrically, most magmatism on Earth occurs by melting of the ultramafic mantle, but this process produces basalts. Making silicic magmas from more mafic parents requires a multi-stage differentiation process. For example, extreme fractionation (>95 % crystal separation) is needed to make granites (Lee and Morton, 2015). Numerous hypotheses have been suggested: crystal settling from more primitive parental magmas, partial melting (anatexis) of pre-existing crust or sediments, compaction-driven crystal segregation, Soret diffusion, zone refining, thermal migration, liquid immiscibility, assimilation of Si-rich sediments or metamorphic wallrocks (Atherton, 1993; Bachl et al., 2001; Bachmann and Bergantz, 2004; Bachmann and Bergantz, 2008; Bacon and Druitt, 1988; Baker and McBirney, 1985; Beard and Lofgren, 1991; Bowen, 1928; Brown, 1994; Brown et al., 1995; Castro, 2013; Castro et al., 2010; Chappell, 1999; Clemens and Stevens, 2012; Glazner et al., 2008; Hildreth, 1979; Hildreth and Wilson, 2007; Jagoutz and Schmidt, 2012; Lipman, 2007; Lundstrom, 2009; McBirney, 1980; Noyes et al., 1983; Philpotts, 1976; Ratajeski et al., 2005; Roedder, 1951; Tuttle and Bowen, 1958; Van Tongeren and Mathez, 2012). To contribute to this topic, we examine a well-exposed tonalitic pluton in which compositions grade from intermediate to high silica contents at the pluton margin. We combine geochemical, petrologic and field observations to determine the mechanism by which the Si-rich boundary layer formed. In this case study, the observations are best explained by compaction-driven segregation of silicic liquids. We combine our observations with thermodynamic models to define the compositional and physical conditions of the magmatic system over which compaction operated.

Study area: Domenigoni Valley pluton, California

The study site is located within the Cretaceous 120 Ma Domenigoni Valley pluton in the northern Peninsular Ranges Batholith in southern California (Morton et al., 2014) (Fig. 1). The pluton comprises a minimum area of ~160 km^2 and intruded into a Jurassic meta-sedimentary

unit composed of meta-greywacke, interlayered calcareous quartzite and phyllite-schist (Morton et al., 2014) (Figs. 1 and 2). The pluton consists of isotropic, medium-grained biotite-hornblende tonalite with accessory zircon, titanite (e.g., sphene), apatite and magnetite-ilmenite. The pluton itself lies within the western zone of the Peninsular Ranges batholith, interpreted to represent juvenile magmas intruded into a Jurassic island arc basement accreted onto the margin of North America (Busby, 2004; Gastil et al., 1988; Gastil, 1975; Kistler et al., 2003; Lee et al., 2007; Morton et al., 2014; Todd et al., 1988). Metamorphic grade of the meta-sediments range from greenschist to amphibolite. Clearly exposed contacts between the metamorphic rocks and the pluton are discordant, as exemplified by truncated metamorphic fabrics (Fig. 2). The presence of porphyritic apophyses emanating into the metamorphic wallrock suggests that the exposed area was structurally near the top of the magma chamber (Morton et al., 2014). Mafic enclaves and metasedimentary xenoliths are common throughout the pluton (Liao et al., 2013; Morton et al., 2014).

We investigated a well-exposed horizontal transect extending 70 m from the wallrock into the pluton (Fig. 2). This transect is exposed along the north side of McCall Blvd. at 33.720391° N and 117.163093° W in the town of Menifee, California (Fig. 1) and is the same transect studied by Turi and Taylor (1971) for oxygen isotopes. Mafic enclaves of igneous origin, but no metasedimentary xenoliths, are found in this transect. We refer in this study to another section of the pluton where metasedimentary xenoliths (pelitic, quartzo-feldspathic and calc-silicate protoliths) are present and in varying states of thermal and chemical equilibration with the pluton (Liao et al., 2013) (Fig. 3a). This outcrop, which we refer to as the "Sun City" locality, is located on the east side of Highway 215 at 33.702514° N and 117.182052° W although it is no longer safe to access (Fig. 1).

Methods

We collected samples along a surveyed transect across the roadcut, taking care to avoid contamination by mafic enclaves. Enclave abundance was estimated visually in 2×2 m squares along the transect. Thin sections were made for selected samples along the transect. The proportions of biotite and hornblende were quantified from scanned thin section images using ImageJ™ software. Whole-rock analyses were completed at the USGS by fusion of powders

105 followed by solution ICP-AES. Mineral chemistries were determined by laser ablation ICP-MS
106 at Rice University (Lee et al., 2009). Data are available in the supplementary tables (Tables A1-
107 A6).
108
109 ## Results
110
111 ### Pluton
112 **Petrography and whole-rock geochemistry.** The pluton is tonalitic and dominated by
113 biotite, hornblende, plagioclase, and quartz. Accessory minerals include apatite, zircon, titanite,
114 and Fe-Ti oxides. Fluid inclusions are abundant in healed fractures of quartz and plagioclase
115 (Fig. 3b), which suggest that the pluton had reached saturation in a free, likely water-rich, fluid
116 phase. Whole-rock major and trace elements of the pluton co-vary in the outer 25 m of the
117 pluton, becoming more silicic and less mafic towards the wallrock contact (Figs. 2c and 4, Table
118 A1): SiO_2 increases from ~68 wt. % in the pluton interior (>25 m) to 75 wt. % at the contact
119 while Mg, Fe, Ca and Co decrease (concentrations reported on a volatile-free basis) (Fig. 4).
120 Mafic mineral abundance (hornblende + biotite), as determined by image analysis of scanned
121 thin sections, decrease from 25 m in the pluton towards the wallrock contact (Fig. 4e). The
122 compositional zonation across the 25 m outer margin yields correlated arrays in element-element
123 variation diagrams (Fig. 5a, b). These correlated arrays can be explained by mixing/unmixing of
124 a hornblende-biotite-plagioclase component (Fig. 5a, b). They do not show any hint of mixing
125 with metasedimentary wallrock.
126 Some whole-rock quantities do not vary across this boundary layer. Previous work (Turi
127 and Taylor, 1971) has shown that whole-rock $\delta_{SMOW}{}^{18}O$ remains constant at ~8 ‰ across this
128 boundary (Fig. 4f), indicating no immediate effect of reaction with or assimilation of the
129 metasedimentary wallrock (19.8 ‰). Whole-rock Zr concentrations are also relatively constant
130 (Table A1; 113 ppm ± 30 ppm (1 σ)). Zr whole-rock concentrations suggest an apparent
131 temperature of ~750 ^{o}C (Fig. 6a, Table A1), assuming the liquid was saturated in zircon
132 (Boehnke et al., 2013; Watson and Harrison, 1983), which is reasonable given that Zr contents of
133 the tonalites as a whole are lower than more intermediate rocks in the Peninsular Ranges
134 Batholith (Lee and Bachmann, 2014). We note that if zircon-saturated magmas contains inherited
135 zircon or excess crystal cargo ("cumulate" zircon), the estimated zircon saturation temperatures

136 are maximum bounds and if they were initially under-saturated, the estimated temperatures are
137 minimum bounds (Miller et al., 2003).
138
139 **Mineral chemistries.** We also analyzed the compositions of plagioclase, biotite and
140 quartz in the pluton across the transect (Tables A4-A6). Plagioclase anorthite varies between 25-
141 35% in a given thin section, but not across the transect (Fig. 6b). In contrast, biotite
142 compositions vary across the 25 m boundary layer: Mg and Co contents of biotite decrease
143 towards the contact, consistent with increasing felsic nature of the bulk rock towards the contact
144 (Fig. 6c). Ti and P contents of quartz show no variation across the transect (Fig. 6d). The Ti
145 contents in the quartz define temperatures of ~580-680 ^{o}C, assuming rutile saturation (Wark and
146 Watson, 2006). Assuming a lower bound of 0.6 for TiO_2 activity gives Ti-in-quartz temperatures
147 of 680-780 ^{o}C. We note that the ~100 ^{o}C variation in temperatures within a given thin section
148 likely reflects sluggish diffusion of Ti rather than analytical uncertainties. Phosphorus, whose
149 concentration in quartz should be buffered by the presence of apatite, is also a sluggish diffusing
150 element, correlating with Ti in quartz (Fig. 6d). The low Ti in quartz temperatures are consistent
151 with the Zr saturation temperatures.
152
153 **Enclaves and xenoliths**
154 **Mafic enclaves from the McCall Boulevard transect.** Mafic enclaves, ranging in size
155 from 5-20 cm, are common in the Domenigoni Valley pluton. These mafic enclaves along the
156 McCall Blvd. transect are amphibole- and biotite-rich, consistent with their more mafic
157 compositions compared to the tonalite (Table A2). They are distinctly different in composition
158 from the metasedimentary xenoliths, described below. In elemental variation diagrams, the
159 McCall Blvd. mafic enclaves define arrays that are complementary to the arrays defined by the
160 tonalites along the transect, suggesting that they may be cumulates associated with the formation
161 of some of the tonalites (Fig. 5a, b). The number density of enclaves across the transect
162 decreases from 5-7.5/m^2 beyond 25 m to none at the contact (Fig. 2c; Table A3). Variation in
163 the spatial abundance of enclaves suggests redistribution by advective or mechanical processes.
164 The coincidence of the spatial variation in enclave abundance and tonalite composition requires
165 that mechanical and chemical processes responsible for differentiating the magma body are
166 coupled.

Metasedimentary xenoliths from the Sun City outcrop. Xenoliths with metasedimentary wallrock protoliths are also present (Fig. 3a, c, d). These are absent from the McCall Blvd. locality but common elsewhere, such as at the Sun City outcrop. In a previous study (Liao et al., 2013; Morton et al., 2014), we showed that the xenolith protoliths are pelites, quartzites and calc-silicates, which underwent varying extents of thermal metamorphism and reactive equilibration with the host tonalitic magma. We discuss these xenoliths briefly for completeness because they are relevant to interpreting the magmatic history. The entire sequence of metamorphic reactions is observed, beginning with calcite- and dolomite-bearing sandstones in the wallrock, followed by thermal metamorphism and decarbonation to wollastonite and diopside after entrainment into the pluton, and ending with transformation of diopside to hornblende with an increase in water activity (and decrease in CO_2 activity). This sequence of reaction is expressed as core to rim variations in mineralogy even in individual xenoliths (Liao et al., 2013). For example, Fig. 3a shows a sample with a diopside-rich core surrounded by a hornblende-rich mantle. Notably, the bulk compositions of different sections of mineralogically zoned xenoliths are relatively constant except for water (Fig. 3c, d). This suggests that, initially, some of these xenoliths were thermally metamorphosed in a closed system except for the rapid diffusion of water into the xenolith. We consider this as indirect evidence that free water permeated the xenoliths and transformed the calc-silicate xenoliths into amphibolites.

Discussion

Si-rich boundary layer generated by crystal-liquid segregation via hindered settling or compaction

The origin of a Si-rich outer boundary layer is perplexing. Cooling of a magma body should initiate from the margins, causing crystallization fronts to migrate inwards and generate margins composed of mafic "cumulates" and plutonic cores of more silicic residual magmas; such zonation is commonly seen in mafic magma bodies (McBirney, 1995; Pitcher, 1997). The outward increase in Si in this study thus seems atypical (Pitcher, 1997), but this reverse zonation may not be that unusual in felsic systems. Felsic plutons with silicic roofs or margins have been

198 reported (e.g., Hutchinson (1956), Fridrich and Mahood (1984), and Allen (1992)). The eruption
199 sequence of ignimbrite deposits often suggest that the top of felsic magma chambers are more
200 silicic (Hildreth and Wilson, 2007). Outer silicic margins are also seen in some nested plutons
201 (Allen, 1992; Coleman et al., 2004). How do these Si-rich boundary layers form?
202 Some scenarios can be ruled out for this particular case study. Local mixing with
203 metasedimentary wallrocks is not evident in any elemental variation diagrams or in the constant
204 oxygen isotopes (Figs. 4 and 5) (but mixing earlier in the magmatic history likely occurred).
205 Soret and thermo-chemical diffusion (Lundstrom, 2009) are inconsistent with the strong spatial
206 coupling between all the elements and the xenolith abundances because elements with different
207 diffusivities should develop boundary layers with different characteristic lengthscales.
208 Coupled chemical and mechanical boundary layers instead require physical segregation
209 of liquids from mineral grains *and* the mafic enclaves. Segregation of mafic minerals, like
210 amphibole and plagioclase can explain the linear arrays in elemental variation diagrams, such as
211 the negative correlation of MgO and CaO with SiO_2. Possible segregation scenarios include
212 compaction-driven expulsion of residual liquids (Bachmann and Bergantz, 2004; Dufek and
213 Bachmann, 2010; McKenzie, 1984; McKenzie, 1987), hindered settling of crystals (Bachmann
214 and Bergantz, 2004), and shear-induced self-diffusion of crystal grains (Barker, 2000; Leighton
215 and Acrivos, 1987; Ross, 1986). Shear-induced flow segregation drives migration of crystal
216 grains away from a high strain boundary layer if there are gradients in crystallinity or effective
217 viscosity perpendicular to large-scale streamlines (Leighton and Acrivos, 1987). If plutons are
218 colder on their margins, higher viscosity and crystallinity on the margins would be expected, so
219 particles might be expected to migrate towards the warmer lower viscosity interior of the magma
220 body owing to asymmetrical inter-grain interactions across the shear boundary layer. However,
221 the migration efficiency (which follows a "diffusive" law) of particles undergoing shear-driven
222 migration should scale with the square of the particle radius, so large particles should migrate
223 farther than small particles (Leighton and Acrivos, 1987). This is not supported by the
224 observation that the abundances of mafic minerals and the much larger mafic enclaves vary over
225 the same lengthscale. Free gravitational settling of crystals also cannot explain the observations
226 because settling velocities similarly scale with the radius squared, causing the transport distances
227 of large particles (enclaves) to differ from mineral grains, which we do not see.

Compaction or hindered settling may be the most plausible mechanism by which coupled mechanical and chemical boundary layers form. Hindered settling occurs at intermediate crystal fractions (20-40%), wherein the separation distance between grains is small enough that differential settling is hindered by viscous interaction between the grains. Compaction occurs by deformation of the crystal mush solid framework and can operate at higher crystal fractions (>40%). In both scenarios, crystal-liquid segregation is driven by differential buoyancy between crystals and liquids, or in the case of compaction, by internal and external stresses as well. The low temperatures (~750 °C) recorded by whole-rock Zr contents and Ti-in-quartz temperatures are well below the liquidus of the tonalitic host, consistent with the granitic boundary layer deriving from a late stage, crystal-rich magma. Depending on the amount of water in the system, crystal fractions at these temperatures can vary from 20 to more than 80%, well within the regime for hindered settling or compaction. Our study provides outcrop confirmation for a compaction origin for the generation of silicic magma bodies (Bachmann and Bergantz, 2004).

Petrogenesis of the silica rich boundary layer

To explore the crystal-liquid segregation scenario further, we used Rhyolite Melts (Gualda et al., 2012) to model crystal-melt equilibria of the host pluton (MR11c at 51.5 m away from the contact; 60-70 wt. % SiO_2) during cooling and crystallization at 3 kbar, corresponding to the average Al-in-hornblende pressures for plutonic rocks in the region (Ague and Brimhall, 1988a; Ague and Brimhall, 1988b). We assume closed system equilibration (batch), that is, liquids and crystallized products are not removed from the system and are always assumed to be in thermal and chemical equilibrium. An oxygen fugacity equivalent to the fayalite-magnetite-quartz buffer was assumed. We modeled melting/crystallization of bulk systems with water contents varying from 0 to 6 wt. % H_2O (Fig. 7).

We compare the modeled geochemical evolution of a crystallizing hydrous tonalite system (6 wt. % H_2O) to the compositions of the mafic enclaves and the tonalite compositions along the McCall Blvd. transect in Fig. 5 (a more detailed discussion on the effects of variable water content are in the next section). Mafic enclaves with SiO_2 between 52-60 wt. % SiO_2 are consistent with being cumulates in equilibrium with the parental tonalitic liquid (69-70 wt. % SiO_2) at model melt fractions of 60-100 %, although it is equally possible that the mafic enclaves represent quenched magmas. The most silicic melts (75 wt. % SiO_2), on the outermost margin of

the pluton, require > 40 % crystallization of the parental tonalite (F<60%), but there are few cumulate xenoliths having compositions in equilibrium with low F (<60%) melts, except for the host tonalite itself. Enclaves with compositions between 60-70 wt. % SiO_2 are absent despite our models predicting their existence if melts were extracted continuously during the crystallization process (Fig. 5c, d). However, at model melt fractions F<20%, hypothetical cumulate compositions in equilibrium with a melt having 75 wt. % SiO_2 are nearly indistinguishable from the parental tonalite in terms of major elements (Fig. 5c, d). Thus, the "cumulate" in equilibrium with the high silica boundary layer may be represented by the host tonalite itself (see also Gelman et al. (2014) and Lee and Bachmann (2015)).

We suggest that the host magma and mafic enclaves were formed together by crystal fractionation of a more primitive magma, presumably at greater depths. The magma then rose into the upper crust, carrying mafic enclaves. After stalling in the upper crust, the magma body cooled and crystallized, generating a crystal-rich mush with a silica-rich residual melt filling the porosity. This Si-rich melt segregated to generate the Si-rich boundary layer, leaving behind a felsic cumulate (likely with intercumulus melt), whose composition is nearly indistinguishable from the parental tonalite itself due to the low melt fractions extracted (Gelman et al., 2014; Lee and Morton, 2015).

Conditions of silicic melt generation and the role of water: observations and thermodynamic models

Insight into the role of water during crystallization of the host tonalite magma can be had from thermodynamic models of melting/crystallization of the host tonalite (MR11c) using Rhyolite Melts (Gualda et al., 2012). Four key effects are noted here:

1) Water changes the temperature interval over which melting occurs (Fig. 7a, b). Liquidus temperatures decrease with increasing dissolved water content (Boettcher and Wyllie, 1968; Castro, 2013). As the magmatic system (crystals + melt) cools and crystallizes, the melt fraction decreases and the water content in the melt increases because water is preferentially partitioned into the melt fraction, which decreases with progressive cooling (Fig. 7c). Water continues to rise until saturation, which at 3 kbar for silicic melts occurs at ~6-7 wt. % H_2O (Fig. 7c). Water concentration in the residual melt scales approximately with the inverse of melt fraction $1/F$ (Jahns and Burnham, 1969). In detail, the inverse relationship with F is of course

modulated by the precipitation of hydrous minerals like amphibole (Jahns and Burnham, 1969). But so long as the system contains reasonable amounts of water (>1 %), saturation is always achieved and all magma bodies can in theory remain molten to minimum melting temperatures (~650 ^{o}C). Systems with high water saturate early (high F), generating large volumes of water-saturated melts, whereas relatively dry systems require extreme fractionation (e.g., when F approaches zero) to achieve saturation.

The above concepts can be restated in the context of melt productivity, *dF/dT*, which describes how much melt *F* is generated per unit increase in temperature *T* (or conversely, how much crystallization occurs per unit decrease in temperature). In a dry system, *dF/dT* is relatively constant, that is, *F(T)* is approximately linear. In a closed, water-rich system, *F(T)* is nonlinear (Fig. 7b): melt productivity, *dF/dT*, is greatest when the system is near or at saturation (Pamukcu et al., 2013). Thus, in water-rich systems, high melt fractions are permissible at near-solidus temperatures, but in water-poor systems, the volume of near solidus melts is small. In part, these effects arise because the evolution of a free fluid phase results in decreased variance of the system, generating eutectic-like behavior, which promotes high melt productivity at the solidus.

2) Water can enhance the SiO_2 (on an anhydrous basis) content of the residual melt because water facilitates the precipitation of amphibole, a low SiO_2-bearing phase (Holloway and Burnham, 1972; Huang and Wyllie, 1986; Kawamoto, 1996), although amphibole is not explicitly modeled in the Rhyolite-Melts modeling we have done. The higher the water content (>1 wt. %), the more amphibole that can precipitate, generating high silica residual melts. Fractionation of a dry tonalite does not generate significant amounts of high silica melts. For example, initial water contents greater than 2 wt. % would generate melts with 75 wt. % SiO_2 after only 20-30 % crystallization (F=70-80%), yielding large quantities of granite (Fig. 7d,e). These initial water contents are relatively modest given that parental basalts in arc environments often already have 4 wt. % H_2O (Plank et al., 2013) and that any subsequent magmatic recharge and crystal fractionation would only increase this value (Lee et al., 2013).

3) Dissolved water in silicate melts decreases melt viscosity by 2 to 3 orders of magnitude (Hui and Zhang, 2007) (Fig. 7f). Thus, during cooling and crystallization of a magma chamber, the viscosity increase of the melt imparted by decreasing temperatures and increasing silica content is counteracted by the decrease in viscosity associated with the ever-increasing

water contents of a diminishing melt fraction (this consideration of viscosity pertains only to the melt, not to the effective viscosity of a crystal+liquid mush). The compensating effect of water on viscosity is most pronounced, as expected, for water-rich systems. This decrease in melt viscosity, as we show below, increases the rate at which melts can be expelled by compaction or hindered settling.

4) Finally, changes in the shape of *F(T)* imparted by water will affect the rate at which latent heat is released (Fig. 7b). We will return to this property later.

Timescales of compaction and hindered settling

Segregating silicic melts from a crystal-rich magma is thought to operate too slowly for sufficient amounts of liquids to be expelled before the magma body freezes (see Jackson et al. (Jackson et al., 2003) for discussion). We begin with the problem of segregating silicic melts from a magma with a crystal volume proportion greater than 30-40 %, corresponding to a porosity of less than 60-70 % (we will treat porosity here as approximately equal to the melt fraction *F*). At intermediate porosities, 60-70%, settling of individual crystals will initially be hindered by viscous interaction with neighboring crystals. As porosity decreases, viscous coupling with neighboring crystals increases the extent that a deformable long-range framework of crystals is formed. And with further decrease in porosity, the framework becomes largely locked, though the framework as a whole can still deform under its own weight or by external stresses. In all these cases, we assume that the crystal-rich magma does not convect because effective viscosities increase by orders of magnitude with increasing crystal volume fraction (decreasing porosity) (Dufek and Bachmann, 2010; Lejeune and Richet, 1995; Mader et al., 2013; Marsh, 1981). We thus treat melt-crystal segregation by hindered settling and compaction, following the spirit of Bachmann and Bergantz (2004).

We first estimate the rates of hindered settling at the top of a crystal-rich suspension, e.g. the magma body, using two empirical approaches. In the first (Richardson and Zaki, 1954; Snabre and Pouligny, 2008), the fall rate V of crystals at the top of the magma body decreases with mean crystal volume fraction χ as (Table 1):

$$V = v(1-\chi)^n \quad (1)$$

where n is ~5 for settling of ideal spheres in purely hydrodynamic interactions (e.g., no electrostatic attractions or surface tension) and v is the Stokes velocity

352 $$v = \frac{2\Delta\rho g R^2}{9\mu} \quad (2)$$

353 where g is gravitational acceleration, $\Delta\rho$ is the difference in density between solid crystals ρ_S
354 and liquid ρ_L, R is the average crystal radius, and μ is the melt viscosity (Pa s). A second
355 formulation, following Bachmann and Bergantz (2004), for hindered settling is given by Barnea
356 and Mizrahi (1973),
357

358 $$V = v\frac{(1-\chi)^2}{\left(1+\chi^{1/3}\right)^{5\chi/3(1-\chi)}} \quad (3)$$

359 where the symbols are the same as defined above. In both equations 1 and 3, when the crystal
360 fraction χ approaches one (or porosity ϕ=*1-*χ approaches zero), settling velocities approach zero.
361 Thus, even though hindered settling also scales with particle radius (see Eq. 2), the differential
362 velocities are slow enough that separation of particles by size will be small. Figure 8 shows
363 some estimates of the timescales for generating silica-rich boundary layers of a given thickness.
364 Taking viscosities for wet (6-7 wt. % H_2O) high silica *liquids* as 10^5 Pa s based on the results of
365 the above Rhyolite MELTS calculations and empirical formulations for viscosity (Hui and
366 Zhang, 2007) and density contrasts between solids and residual liquids during the last stages of
367 crystallization of 300 kg/m^3, it can be seen that at porosities between 0.2-0.5 and a grain size of
368 ~3 mm, it would take ~10 ky to expel 25 m of Si-rich granitic melt and ~10-100 ky to expel 500
369 m of melt. Because settling velocity scales inversely with viscosity of the liquid, increasing the
370 viscosity to 10^6 to reflect less hydrous magmas would increase timescales of expulsion to 0.1-1
371 My.
372 Given that crystal grains are likely to form a penetrative, but porous framework at
373 porosities lower than ~0.5-0.7 (Mooney, 1951; Saar et al., 2001; Scott and Kohlstedt, 2006),
374 compaction may be a better description of melt segregation than hindered settling. We consider
375 the case in which a porous crystal-rich mush (the magma chamber) rests on top of an
376 impermeable boundary at its base. The mush compacts under its own weight, with the basal
377 portions compacting first (decreasing porosity), driving expulsion of the interstitial melt through
378 the top of the magmatic mush. The flow of melt relative to the compacting crystal matrix can be
379 described by Darcy flow, wherein the pressure gradient is driven by the buoyancy difference

between crystals and melt. Melt velocity is zero at the base but increases upwards, reaching a constant upward velocity if the scale height of the magma body is significantly larger than the compaction lengthscale, which is the lengthscale over which the crystal framework compacts. The compaction lengthscale δ_c is given by

$$\delta_c = \left[\frac{\varsigma + 4\eta/3}{\mu} k_\phi \right]^{1/2} \quad (4)$$

where ζ and η are the effective bulk and shear viscosities of the matrix, μ is the viscosity of the melt, and k_ϕ is the permeability, all of which depend on porosity ϕ (McKenzie, 1984; McKenzie, 1987). For spherical grains, permeability can be approximated as (Bear, 1972; Carman, 1937; Kozeny, 1927)

$$k_\phi = \frac{R^2 \phi^3}{180(1-\phi)^2} \quad (5)$$

For porosities between 0.2-0.6 and grain radii of ~3 mm, k_ϕ is on the order of 10^{-8} to 10^{-9} m^2. Effective bulk and shear viscosities of the matrix are difficult to determine, but for porosities >0.3, might be on the order of 10^{13} to 10^{15} Pa s (Bachmann and Bergantz, 2004; Jackson et al., 2003; Rabinowicz et al., 2001). Using a representative melt viscosity of ~10^5 Pa s for a hydrous Si-rich melt (Fig. 7f) yields compaction lengthscales <1 m for magmatic mushes (using higher melt viscosities would further decrease the compaction lengthscale). Given that the scale height of the magma chamber is on lengthscales of km and, hence, much greater than any compaction lengthscale, the relative velocity w_o between the melt and crystal framework at the top of the magma body can be approximated by Darcy flow

$$w_o = \frac{k_\phi (1-\phi) \Delta \rho g}{\mu \phi} \quad (6)$$

The actual rate at which a crystal-free melt layer thickens at the top of magma body is $w_o\phi$. For porosities between 0.2-0.4, we find that a 25 m thick layer requires 1-10 ky to form and a 500 m thick layer requires ~100 ky (Fig. 8). In all cases, if we adopt a viscosity of 10^6 Pa s, timescales for extraction increase ten-fold. We note that our simplified approach in estimating the thickness of the extracted melt layer by compaction assumes that the height of the magma chamber is much larger than the compaction lengthscale. Our approach differs from that of Bachmann and Bergantz (2004). They estimated the characteristic time over which the melt in the magma chamber is drained by e-fold (e.g., by ~1/2.7). This not only requires assuming a magma

chamber size, which is not known, but also assumes that silicic boundary layers are formed only after e-fold drainage of the melt. Recent work shows that most plutons do not efficiently drain (Lee and Morton, 2015).

Magma chamber lifespan and the role of water and latent heat

Can a magma body remain partially molten long enough for compaction/hindered settling to occur? The lifespan of a magma body depends on the efficiency of heat loss and gain. Heat loss rates depend on the nature of heat transfer (magma convection, conduction, or hydrothermal circulation in the country rock) and the thermal state of the country rock. Heat gain occurs by magmatic recharge and release of latent heat (Gelman et al., 2013; Marsh, 1981). Release of latent heat applies to all crystallizing magma bodies, but how latent heat is released during the crystallization interval (from liquidus to solidus) may play an important role in the formation and segregation of silica-rich melts. To illustrate, we first consider the general case of constant latent heat release over the crystallization interval (e.g., constant melt productivity) for a non-convecting magma body. In this case, the thermal evolution of the magma body can be modeled by heat diffusion

$$\rho_m c \frac{\partial T}{\partial t} + \rho_m L \frac{\partial F}{\partial T}\frac{\partial T}{\partial t} = -k\nabla^2 T \quad (7)$$

where ρ is density (kgm^{-3}), c is the specific heat ($Jkg^{-1}°C^{-1}$), T is temperature (°C), t is time, k is thermal conductivity ($Wm^{-1}°C^{-1}$), F is the liquid fraction (which varies from 0 at the solidus temperature to 1 at the liquidus temperature), and $\partial F/\partial T$ is the melt productivity per unit increase in T. L is the *total* latent heat released (Jkg^{-1}) between the liquidus and solidus temperatures. If $\partial F/\partial T$ is constant over a particular temperature interval, then non-dimensionalizing Equation 7 results in the following expression for the characteristic diffusion time for a cooling magma body

$$t \sim \frac{x^2}{\kappa}\left(1 + \frac{L}{c}\frac{\partial F}{\partial T}\right) \quad (8)$$

where x is the characteristic size (e.g., radius) of the magma body and κ is the thermal diffusivity ($k/(\rho c)$). If $L = 0$, Eq. 8 simplifies to the conventional thermal diffusion timescale $t \sim x^2/\kappa$. For typical values of total L (40 kJ/kg) (Lange et al., 1994), c (1000 $Jkg^{-1}°C^{-1}$), and κ (10^{-6} m^2/s) and assuming a 300 °C melting interval over which $F(T)$ is perfectly linear, the second term in

parentheses is ~1.3, which means that the release of latent heat increases the lifespan of a magma body by a factor of ~2.

The problem becomes more interesting when we consider *F(T)* to be nonlinear as shown above. Based on the Rhyolite MELTS model outputs (Fig. 7a, b), we parameterize F with a 6th order polynomial (Table A7)

$$F = \sum_{i=1}^{6} a_i \overline{T}^i \quad (9)$$

where temperature is normalized to the difference between the liquidus temperature T_L and solidus temperature T_S:

$$\overline{T} = \frac{T - T_S}{T_L - T_S} \quad (10)$$

T_s, T_L and the curvature of *F(T),* as expressed in terms of the polynomial coefficients a_i, depend on bulk composition and pressure (for the purposes of this study, we assume one bulk composition and pressure of 3 kbar). To predict melt compositions, we also parameterized our Rhyolites MELTS-modeled SiO_2 concentrations of the melt (on an anhydrous basis) as a function of temperature with a 6th order polynomial (Table A7)

$$SiO_2(melt) = \sum_{i=0}^{6} b_i \overline{T}^i \ . \quad (11)$$

In water-bearing systems, progressive crystallization causes the residual liquid's dissolved water content to increase, eventually leading to saturation in a free fluid (water) phase. When a free fluid phase appears, the thermodynamic variance of the system decreases, causing the system to behave like a eutectic (Vielzeuf and Schmidt, 2001) so that melt productivity is highest just above the solidus. Under dry conditions, the eutectoid behavior is reduced, which is manifested as near constant melt productivity (*dF/dT*) or linear F over the melting interval. By contrast, the nonlinearity in *F(T)* in water-bearing systems delays the release of latent heat and hence the bulk of the crystallization to late in a magma body's thermal life. For example, for a bulk water content of 6 wt. %, 80% of the crystallization and release of latent heat is delayed to temperatures within 20% of the solidus ($\overline{T}$ <0.2) (Fig. 7b), consistent with experimental results (Marsh, 1981; Pamukcu et al., 2013; Scaillet et al., 1997). By contrast, for relatively dry systems (0.3 wt. % H_2O), 90% of the magma crystallizes at temperatures well above the solidus ($\overline{T}$ >0.2) (Fig. 7b). The extent to which crystallization is delayed correlates with bulk water content

because higher bulk water contents cause fluid saturation to occur at higher normalized temperatures and higher melt fractions, F.

To apply these concepts, we solved Equation 7 for a variable dF/dT by forward finite difference using the following formula to calculate temperature at time step j

$$T_{i,j+1} = \left(\frac{-\kappa}{1+(dF/dT)L/c} \right) \left[\frac{T_{i+1,j} - 2T_{i,j} + T_{i-1,j}}{\Delta x^2} \right] \Delta t + T_{i,j} \quad (11)$$

where i is the spatial index, Δt is the time increment, and Δx is the spatial increment. Initial temperature of the magma body was taken to be the liquidus temperature, which varies with water content. We adopted a total latent heat L of 40 kJ/kg (Lange et al., 1994) and assumed this value to be constant regardless of water content, which we confirmed using the MELTS model outputs. The initial wall rock temperature was set at 400 ^{o}C. A typical thermal diffusivity of 10^{-6} m/s^2 was assumed. We assumed that the magma body was tabular in shape and that the smallest dimension is its thickness. Although we do not know the thickness of the magma body, we assume a value of 5 km to approximate a pluton that extends throughout the upper crust (based on Al-in-hornblende barometry from Ague and Brimhall (1988b)). Temperature-dependency on thermal diffusivity would increase magma lifespan slightly (Gelman et al., 2013; Whittington et al., 2009), but was ignored here to isolate the effect of latent heat. In addition to ignoring magma convection, we have also ignored hydrothermal circulation, both of which would hasten the cooling of the magma body.

Our thermal models are shown in Fig. 9. The lifespan (time above solidus) of a single-stage magma body emplaced into the upper crust and conductively cooled without latent heat ($L=0$) is ~0.4 My (Fig. 9b). This is just long enough for a liquid boundary layer of 25 m to segregate by compaction. When latent heat is considered, regardless of the amount of system water content, the characteristic cooling times of tonalitic magmas are 0.8 My, as predicted from simple scaling (Eq. 8). This increase in cooling time allows for a much thicker boundary layer to form. However, the most interesting effect is that water modulates the amount of time the magma body spends at near solidus conditions and the amount of water-rich, high silica melts that can be generated (Fig. 9c). Wet magmas that reach water saturation early will delay most of the crystallization to near solidus temperatures, causing prolonged thermal arrest at the temperatures and melt fractions in which high silica residual liquids are generated. As can be seen in Fig. 9d, wet magmas generate more silica-rich melts during their lifespans while the

494 delayed release of latent heat in water-bearing systems, prolongs the relative time interval over
495 which silicic liquids can be expelled.
496
497 **What is the importance of water in generating granites?**
498 Our observations on the generation and extraction of silicic magmas may have more
499 general implications for making silicic melts, such as granite. Numerous studies have argued that
500 granite formation requires water and that because Earth has water, it has granites and continents
501 (Campbell and Taylor, 1983; Rosing et al., 2006; Watson and Harrison, 2005). For instance,
502 although granites can be found in relatively dry magmatic systems, such as at spreading ridges
503 and hotspots on Earth (Carmichael, 1964) and even on the Moon (Bonin, 2012; Warren et al.,
504 1983), the volume of such granites is negligible compared to the volumes of granites found in
505 subduction zones where water is available from the parental basalts. There is no debate that the
506 formation of large volumes of granite requires water, but the importance of water is often
507 confused.
508 The standard view is that because water reduces the melting point of rocks and makes it
509 easier to heat rocks to their melting points (Patino Douce and Johnston, 1991; Vielzeuf and
510 Schmidt, 2001), hence granites mostly form by up-temperature processes, that is, by partial
511 melting of pre-existing crust (crustal anatexis) rather than by down-temperature crystallization
512 from a hot, more primitive magma. Low zircon crystallization temperatures (700 °C) inferred
513 from Ti contents of zircon have occasionally been argued to indicate an origin by water-saturated
514 partial melting (Watson and Harrison, 2005). However, metasediments or metabasalts do not
515 typically have enough bound water to always melt under water-saturated conditions (Rutter and
516 Wyllie, 1988). Melting the crust requires heat, which commonly comes from intrusion or
517 underplating of hot magmas like basalts for crustal and upper mantle thermal states typical of
518 most of Earth's history (Dufek and Bergantz, 2005; Jackson et al., 2003; Rutter and Wyllie,
519 1988), but it has been shown that such heating is inefficient in producing significant amounts of
520 anatexis (Dufek and Bergantz, 2005). There is, of course, no doubt that some types of granitoids
521 form by melting of metasediments (Chappell, 1999; Chappell et al., 1992), but whether the
522 majority granites form by anatexis is debated.
523 Here, we argue that any moderately hydrous (>2 wt. %) parental magma will reach water
524 saturation and minimum melting temperatures by crystal fractionation during cooling or

525 decompression during ascent (Albarede, 1983; Cann, 1970). Thus, the ubiquity of granites can be
526 explained if granites dominantly form by down-temperature crystal fractionation of hydrous
527 magmas. This view is similar to that in other studies based on indirect constraints from
528 ignimbrite stratigraphy or from magma Zr concentrations that suggest higher temperatures than
529 that inferred from Ti in zircon thermometry (Gelman et al., 2013; Hildreth, 1979; Hildreth and
530 Wilson, 2007; Lee and Bachmann, 2014; Miller et al., 2003; Wade et al., 2005). Most trace-
531 element or isotopic signatures indicative of crustal assimilation are likely inherited from more
532 mafic and hence parental magmas that assimilated crust in deep crustal magmatic zones, where
533 background temperatures are high, making it easier to assimilate the wallrock (Annen et al.,
534 2006; Hildreth and Moorbath, 1988).
535
536 **Summary: prospects and limitations of making high silica magmas by crystal fractionation**
537
538 We show from a unique outcrop that silicic melts can form by compaction driven
539 segregation from a partially crystallized intermediate magma, confirming other studies based on
540 geochemical systematics (Bachmann and Bergantz, 2004; Bachmann and Bergantz, 2008; Lee
541 and Bachmann, 2014; Putirka et al., 2007). We suggest that granites can be readily formed by
542 crystal-fractionation from intermediate magmas undergoing compaction or hindered settling,
543 though we cannot draw from our study whether such processes are dominant. Nevertheless, we
544 envision the following scenario for the formation of granites. Mantle-derived hydrous basalts rise
545 into the lower crust, where they stall and cool. Crystal fractionation generates deep crustal mafic
546 cumulates and intermediate residual magmas (andesites to dacites) (Canil et al., 2010; DeBari
547 and Sleep, 1991; Ducea, 2001; Ducea, 2002; Greene et al., 2006; Hacker et al., 2008; Hildreth
548 and Moorbath, 1988; Jagoutz and Schmidt, 2012; Jagoutz, 2010; Lee et al., 2006; Lee et al.,
549 2012; Lee et al., 2007). These intermediate magmas then ascend into the upper crust, carrying a
550 cargo of mafic enclaves (Barbarin, 2005; Barbarin et al., 1989; Farner et al., 2014; Paterson et
551 al., 1989). These intermediate magmas continue to cool and crystallize, causing residual melts to
552 become more water- and silica-rich. The Si-rich melts are expelled from the intermediate
553 magma mush, generating Si-rich boundary layers at the tops of the magma bodies. The
554 remaining magmatic mush crystallizes into a pluton, which, by definition, is the adcumulate
555 (crystals + interstitial trapped liquid) complement to the high silica melt (conceptually, this

adcumulate/restite is similar to that described in (Langmuir, 1989)). Because of the small amounts of melts formed, the composition of this cumulate pluton should be nearly indistinguishable from that of an intermediate parental magma itself, especially if there is trapped melt (Lee and Morton, 2015). This may explain why granitoid plutonic rocks appear to have compositions that can be modeled as silicate liquids but at the same time have textures suggestive of a cumulate origin (Vernon, 1986). There is some potential for using trace elements to help distinguish silicic cumulates from silicic melts (Deering and Bachmann, 2010; Gelman et al., 2014; Lee and Morton, 2015).

In summary, down-temperature crystal fractionation of more mafic, hotter parents to form granites is a viable process (Bowen, 1915; Bowen, 1928; Bucholz et al., 2014; Deering and Bachmann, 2010; Jagoutz and Schmidt, 2012; Jagoutz, 2010; Lee and Bachmann, 2014). Water significantly enhances the efficiency of making granites because it lowers melt viscosity, increases silica activity, and suppresses much of the crystallization to late in the thermal life of the magma where water and silica activity are greatest. The latter effect prolongs the lifespan of the magma at the time in which silicic melts are being produced, allowing more time for extraction from the crystal mush by hindered settling or compaction. However, simple mass balance shows that the total amount of granite that can be generated from a basaltic parental magma is ultimately small (<5 % of original mass of basalt), consistent with the observation that only small volumes of granites are found in volcanic arcs (Lee and Morton, 2015; Putirka et al., 2014).

Acknowledgments. We thank Tien Chang Lee, Helge Gonnermann, Olivier Bachmann, Monica Erdman, and Michael Manga for discussions. Guilherme Gualda, Jonathan Miller and Calvin Miller are thanked for insightful reviews. This work was supported by NSF OCE-1338842.

Table 1. List of parameters and symbols

Symbol	Definition	units
V	hindered settling velocity	m/s
ν	Stoke's settling velocity	m/s
χ	crystal volume fraction in magma	
ϕ	porosity	
$\Delta\rho$	density difference between crystals and melt	kg/m^3

ρ_m	density of magma body	kg/m^3
ρ_L	density of silicate liquid	kg/m^3
ρ_s	density of solids	kg/m^3
g	gravitational acceleration	m/s^2
R	crystal radius	m
δ_c	compaction lengthscale	m
k_ϕ	permeability	m^2
F	melt fraction	
dF/dT	melt productivity	°C^{-1}
μ	viscosity of silicate liquid (melt)	Pa s
ζ	effective bulk viscosity of crystal matrix	Pa s
η	effective shear viscosity of crystal matrix	Pa s
w_o	relative velocity between melt and crystals at top of crystal mush	m/s
T	temperature	°C
T_S	solidus temperature	°C
T_L	liquidus temperature	°C
$\overline{T}$	dimensionless temperature	
t	time	s
Δt	time increment	°C
L	total latent heat	J/kg
c	specific heat	J/kg°C
k	thermal conductivity	W/m°C
κ	thermal diffusivity (=$k/\rho c$)	m/s^2
x	distance	m
C_o	weight concentration of element in system	
a_i	constants for polynomial fit of $F\left(\overline{T}\right)$	
b_i	constants for polynomial fit of $F\left(\overline{T}\right)$	

Supplementary Tables

Table A1. Whole-rock major and trace elements of host tonalite and wallrock
Table A2. Whole-rock major and trace elements of mafic xenoliths
Table A3. Xenolith frequency along McCall Blvd.
Table A4. Quartz composition in tonalite
Table A5. Biotite composition in tonalite
Table A6. Plagioclase composition in tonalite
Table A7. Empirical parameterizations for melting models

Fig. 1. Location map of the Domenigoni Valley Pluton. Study area of the McCall Blvd. transect in Fig. 2 is labelled. Sun City outcrop where metasedimentary xenoliths have been previously studied (Liao et al., 2013) is also shown.

Fig. 2. Photograph of the roadcut along McCall Boulevard in Menifee (formerly Sun City), California (33°43'13,32" N; 117°09'46.94" W) with Toyota Prius™ for scale at far left. Wallrock (WR) contact with pluton is denoted by vertical dashed line. Insets above A) show close up views of the contact and the pluton along with examples of mafic enclaves. B) Photomicrograph thin sections in plane light sampled at different distances from the contact (numbers represent meters). Brown minerals are hornblende and biotite; clear minerals are quartz and feldspars. C) Plot of the number of enclaves per 2×2 m square (left axis) and bulk rock MgO content of the pluton (excluding enclaves) are plotted with distance from the contact.

Fig. 3. A) Zoned calc-silicate metasedimentary xenolith (sample SC-7 from (Liao et al., 2013)) from Sun City location in the Domenigoni Valley pluton. Di = diopside, Qz = quartz, Fsp = feldspar, Hb = hornblende. B) Fluid inclusions in healed fractures in quartz within the tonalite pluton at McCall Blvd.. C and D) Compositions of metasedimentary xenoliths from Sun City location (Liao et al., 2013). Samples from the same xenolith but different sections of the xenolith share identical colored symbols. Sample SC-7 from A) is shown. Limited intra-xenolith compositional variation is seen, suggesting isochemical transformation with the exception of the ingress of water to convert diopside to hornblende.

679
680 **Fig. 4.** Compositional transects across the contact and into the pluton at McCall Blvd. Plutonic
681 rocks are represented by solid black circles. Wallrock represented by open squares. A-D) show
682 SiO_2, MgO, TiO_2 and Co versus distance; oxides are in wt. %, but Co is in ppm by weight. E)
683 Modal percent of biotite+hornblende in the pluton as estimated by image analysis of thin
684 sections. F) Whole-rock oxygen isotopic (‰ deviation from SMOW) composition from Turi and
685 Taylor (Turi and Taylor, 1971).
686
687 **Fig. 5**. A and B) show MgO and CaO versus SiO_2 (wt. % on anhydrous basis) of the pluton
688 (yellow circles) and mafic enclaves (green squares) from the McCall Blvd. transect. Wallrocks
689 and metasedimentary xenoliths from McCall Blvd. and Sun City locations, respectively, are
690 shown as small open circles. Green and red lines represent isobaric (3 kbar) closed system
691 Rhyolite-MELTS models for the liquid (red) and crystal (green) lines of descent of a parental
692 tonalite composition at 55 m from the contact and an assumed system water content of 6 wt. %.
693 Arrows indicate direction of cooling and decreasing residual melt fraction. In A, dashed arrowed
694 lines point towards mineral endmembers. C and D) SiO_2 and MgO (wt. % on anhydrous basis) of
695 model residual liquid formed during crystallization of the parental tonalite plotted as a function
696 of residual melt fraction F. Color of lines correspond to the same as in A and B. Compositions
697 of melt and cumulate in equilibrium are shown with tie lines. Stage 1 cumulates could be
698 represented by the mafic enclaves in the McCall Blvd. transect and can be seen here to be in
699 equilibrium with the parental tonalite, suggesting that the mafic enclaves may represent cognate
700 cumulate xenoliths entrained as cargo in the parental tonalite when it rose and became emplaced
701 into the upper crust. There is a distinct absence of enclaves having compositions between ~62-
702 70 wt. % SiO_2 despite model results that predict such lithlogies should have formed. Final
703 extraction of Si-rich melts (75 wt. %) leaves behind a "cumulate" with approximately the same
704 composition of the parental tonalite. We refer to these cumulates as stage 2 cumulates.
705 Crystallization models are done using Rhyolite-Melts (Gualda et al., 2012).
706
707 **Fig. 6.** A) Various estimates of magmatic temperatures from McCall Blvd. transect plotted
708 versus distance from contact. Red symbols are apparent Zr saturation temperature as inferred
709 from whole-rock Zr contents and Zr solubility models (Watson and Harrison, 1983). Circles
710 represent Ti-in-quartz temperatures assuming TiO_2 activities of 1 (open symbols) and 0.6 (black
711 symbols). B) Plutonic plagioclase Anorthite content in pluton versus distance. C) Plutonic
712 biotite Co (ppm; black circles) and MgO (wt. %; open squares) concentrations versus distance.
713 D) Ti and P elemental concentrations (ppm) in plutonic quartz.
714
715 **Fig. 7**. Thermodynamic models of liquid lines of descent from a parental tonalite having a
716 composition equal to the tonalite at ~50 m inward of the pluton margin. A) Melt fraction (*F*) as a
717 function of temperature for different bulk system water contents (H_2O_i) based on Rhyolite Melts
718 modeling (Gualda et al., 2012; Pamukcu et al., 2013). Lines are colored for different bulk water
719 contents. B) Same as in A but temperature has been re-normalized to the temperature difference
720 between the solidus and the liquidus. C) H_2O wt. % in the residual melt as a function of
721 temperature. H_2O contents rise with cooling because H_2O behaves as an incompatible element.
722 D) SiO_2 (wt. %) in the residual melt versus temperature. E) SiO_2 (wt. % on anhydrous basis) in
723 the residual melt versus melt fraction F. H_2O concentrations are bounded by the saturation
724 curve. F) Viscosity of the melt (Pa s) plotted versus temperature of the system. Note that this is

not a plot showing how temperature influences melt viscosity. These curves are controlled by a combination of H_2O, temperature, and melt composition, all of which change during crystallization. SiO_2 contents for melt fractions below ~15 % are not reported.

Fig. 8. Time to generate a 25 m thick silicic boundary layer by hindered settling (A, B) and compaction (C). A and B correspond to two different treatments of hindered settling. D-F) are the same as A-C except they represent the time to generate a 500 m thick boundary layer. Horizontal axis in all plots represents porosity, which is approximately equal to the melt fraction. Crystal radius of 3 mm and density contrast of 300 kg/m^3 are assumed. Curves in each plot correspond to different viscosities ($\log_{10}\mu$ in Pa s).

Fig. 9. A) Thermal evolution of a 5 km thick tabular magma body intruded into a country rock with a background temperature of 400 ^{o}C. Initial temperature of the magma is assumed to correspond to its liquidus, which we assume here to correspond to a tonalitic liquid with 4 wt. % H_2O. Temperature profiles for different times are shown. Thermal model assumes thermal conduction with the effect of latent heat, but convection is ignored. Dashed line represents initial condition. B) Temperature of the center of the magma body as a function of time for systems with different bulk water contents (closed system is assumed). Initial temperature of the magma corresponds to liquidus temperature at relevant water content. Each colored line represents a model for different bulk water contents. All models assume a constant total latent heat, but different functional forms of $F(\overline{T})$. Black curved line corresponds to the unrealistic scenario where total latent heat is zero. C) Melt fraction at the center of the cooling magma body as a function of time. D) SiO_2 content of the residual liquid as a function of time. SiO_2 contents for melt fractions less than ~15 % are not reported.

Fig. 10. Hypothetical model for the formation of granites by crystal-liquid segregation. Stage 1. An intermediate magma (60-70 wt. % SiO_2) is generated in a deep crustal magma chamber by crystal fractionation of a more primitive and mafic parent. The intermediate magma is evacuated from the deep crustal magma chamber, entraining some of its own cumulates (mafic enclaves). This intermediate magma along with its cumulate cargo is emplaced in the shallow crust. In Stage 2, the magma body cools isobarically. Residual liquids rich in water and silica form with progressive crystallization. Residual liquids are expelled to the sides and roof of the magma body by compaction and/or hindered settling, generating a crystal-poor silicic boundary layer. The crystal-rich mush represents a restite/cumulate of the silicic melt in the boundary layer.

References

Ague, J.J., and Brimhall, G.H. (1988a) Magmatic arc asymmetry and distribution of anomalous plutonic belts in the batholiths of California: effects of assimilation, crustal thickness and depth of crystallization. Geological Society of America Bulletin, 100, 912-927.

-. (1988b) Regional variations in bulk chemistry, mineralogy, and the compositions of mafic and accessory minerals in the batholiths of California. Geological Society of America Bulletin, 100, 891-911.

771 Albarede, F. (1983) Limitations thermiques a l'ascension des magmas hydrates. Comptes Rendus de
772 l'Académie des Sciences, 296, 1441-1444.
773 Allen, C.M. (1992) A nested diapir model for the reversely zoned Turtle Pluton, southeastern California.
774 Transactions of the Royal Society of Edinburgh, Earth Science, 83, 179-190.
775 Annen, C., Blundy, J.D., and Sparks, R.S.J. (2006) The genesis of intermediate and silicic magmas in deep
776 crustal hot zones. Journal of Petrology, 47, 505-539.
777 Atherton, M.P. (1993) Granite magmatism. J. Geol. Soc. London, 150, 1009-1023.
778 Bachl, C.A., Miller, C.F., Miller, J.S., and Faulds, J.E. (2001) Construction of a pluton: evidence from an
779 exposed cross-section of the Searchlight pluton, Ledorado Mountains, Nevada. Geological
780 Society of America Bulletin, 113, 1213-1228.
781 Bachmann, O., and Bergantz, G.W. (2004) On the origin of crystal-poor rhyolites: extracted from
782 batholithic crystal mushes. Journal of Petrology, 45, 1565-1582.
783 -. (2008) Rhyolites and their source mushes across tectonic settings. Journal of Petrology, 49, 2277-2285.
784 Bacon, C.R., and Druitt, T.H. (1988) Compositional evolution of the zoned calcalkaline magma chamber
785 of Mount Mazama, Crater Lake, Oregon. Contributions to Mineralogy and Petrology, 98, 224-
786 256.
787 Baker, B.H., and McBirney, A.R. (1985) Liquid fractionation. Part III: geochemistry of zoned magmas and
788 the compositional effects of liquid fractionation. Journal of Volcanology and Geothermal
789 Research, 24, 55-81.
790 Barbarin, B. (2005) Mafic magmatic enclaves and mafic rocks associated with some granitoids of the
791 central Sierra Nevada batholith, California: nature, origin, and relations with the hosts. Lithos,
792 80, 155-177.
793 Barbarin, B., Dodge, F.C.W., Kistler, R.W., and Bateman, P.C. (1989) Mafic inclusions, aggregates and
794 dikes in granitoid rocks, central Sierra Nevada batholith, California - Analytic data. United States
795 Geological Survey Bulletin, 1899, 28.
796 Barker, D.S. (2000) Emplacement of a xenolith-rich sill, Lajitas, Texas. Journal of Volcanology and
797 Geothermal Research, 104, 153-168.
798 Bear, J. (1972) Dynamics of fluids in porous media. Elsevier Publications.
799 Beard, J.S., and Lofgren, G.E. (1991) Dehydration melting and water-saturated melting of basaltic and
800 andesitic greenstones and amphibolites at 1, 3, and 6.9 kbar. Journal of Petrology, 32, 365-401.
801 Boehnke, P., Watson, E.B., Trail, D., Harrison, T.M., and Schmitt, A.K. (2013) Zircon saturation re-
802 revisited.
803 Boettcher, A.L., and Wyllie, P.J. (1968) Melting of granite with excess water to 30 kilobars pressure.
804 Journal of Geology, 76, 235-244.
805 Bonin, B. (2012) Extra-terrestrial igneous granites and related rocks: a review of their occurrence and
806 petrogenesis. Lithos, 153, 3-24.
807 Bowen, N.L. (1915) The crystallization of haplodioritic, and related magmas. Amer. J. Sci., 40, 161-185.
808 -. (1928) The evolution of the igneous rocks. 334 p. Princeton University Press, Princeton, New Jersey.
809 Brown, M. (1994) The generation, segregation, ascent and emplacement of granitic magma: the
810 migmatite-to-crustally derived granite connection in thickened orogenies. Earth Sci. Rev., 36, 83-
811 130.
812 Brown, M., Averkin, Y.A., and McLellan, E.L. (1995) Melt segregation in migmatites. Journal of
813 Geophysical Research, 100, 15655-15679.
814 Bucholz, C.E., Jagoutz, O., Schmidt, M.W., and Sambuu, O. (2014) Fractional crystallization of high-K arc
815 magmas: biotite- versus amphibole-dominated fractionation series in the Dariv Igneous
816 complex, Western Mongolia. Contributions to Mineralogy and Petrology, 168, 1072.
817 Busby, C. (2004) Continental growth at convergent margins facing large ocean basins: a case study from
818 Mesozoic convergent-margin basins of Baja California, Mexico. Tectonophysics, 392, 241-277.

819 Campbell, I.H., and Taylor, S.R. (1983) No Water, No Granites - No Oceans, No Continents. Geophysical
820 Research Letters, 10(11), 1061-1064.
821 Canil, D., Styan, J., Larocque, J., Bonnet, E., and Kyba, J. (2010) Thickness and composition of the
822 Bonanza arc crustal section, Vancouver Island, Canada. Geological Society of America Bulletin.
823 Cann, J.R. (1970) Upward movement of granitic magma. Geological Magazine, 107, 335-340.
824 Carman, P.C. (1937) Fluid flow through a granular bed. Transactions of the Institute of Chemical
825 Engineering, London, 15, 150-156.
826 Carmichael, I.S.E. (1964) The petrology of Thingmuli, a tertiary volcano in Eastern Iceland. Journal of
827 Petrology(435-460).
828 Castro, A. (2013) Tonalite-granodiorite suites as cotectic systems: a review of experimental studies with
829 applications to granitoid petrogenesis. Earth-Science Reviews, 124, 68-95.
830 Castro, A., Gerya, T., García-Casco, A., Fernández, C., Déaz-Alvarado, J., Moreno-Ventas, I., and Löw, I.
831 (2010) Melting relations of MORB-sediment mélanges in underplated mantle wedge plumes;
832 implications for the origin of Cordilleran type batholiths. Journal of Petrology, 51, 1267-1295.
833 Chappell, B.W. (1999) Alumina saturation in I- and S-type granites and the characterization of
834 fractionated haplogranites. Lithos, 49, 535-551.
835 Chappell, B.W., White, A.J.R., and Brown, P.E. (1992) I- and S-type granites in the Lachlan fold belt.
836 Transactions of the Royal Society of Edinburgh, Earth Science, 83, 1-26.
837 Clemens, J.D., and Stevens, G. (2012) What controls chemical variation in granitic magmas? Lithos, 134-
838 135, 317-329.
839 Coleman, D.S., Gray, W., and Glazner, A.F. (2004) Rethinking the emplacement and evolution of zoned
840 plutons: geochronologic evidence for incremental assembly of the Tuolumne Intrusive Suite,
841 California. Geology, 32, 433-436.
842 DeBari, S.M., and Sleep, N.H. (1991) High-Mg, low-Al bulk composition of the Talkeetna island arc,
843 Alaska: implications for primary magmas and the nature of arc crust. Geological Society of
844 America Bulletin, 103, 37-47.
845 Deering, C.D., and Bachmann, O. (2010) Trace element indicators of crystal accumulation in silicic
846 igneous rocks. Earth and Planetary Science Letters, 297, 324-331.
847 Ducea, M. (2001) The California arc: thick granitic batholiths, eclogitic residues, lithosphere-scale
848 thrusting, and magmatic flare-ups. Geological Society of America Today, 11, 4-10.
849 Ducea, M.N. (2002) Constraints on the bulk composition and root foundering rates of continental arcs: a
850 California arc perspective. Journal of Geophysical Research, 107, doi:10.1029/2001JB000643.
851 Dufek, J., and Bachmann, O. (2010) Quantum magmatism: magmatic compositional gaps generated by
852 melt-crystal dynamics. Geology, 38, 687-690.
853 Dufek, J., and Bergantz, G.W. (2005) Lower crustal magma genesis and preservation: a stochastic
854 framework for the evaluation of basalt-crust interaction. Journal of Petrology, 46, 2167-2195.
855 Farner, M.J., Lee, C.-T.A., and Putirka, K.D. (2014) Mafic-felsic magma mixing limited by reactive
856 processes: a case study of biotite-rich rinds on mafic enclaves. Earth and Planetary Science
857 Letters, 393, 49-59.
858 Fridrich, C.J., and Mahood, G. (1984) Reverse zoning in the resurgent intrusions of the Grizzly Peak
859 cauldron, Sawatch Range, Colorado. Geological Society of America Bulletin, 95, 779-787.
860 Gastil, G., Morgan, G., and Krummenacher, D. (1988) The tectonic history of Peninsular California and
861 adjacent Mexico. In W.G. Ernst, Ed. Metamorphic and tectonic evolution of the Penisular Ranges
862 batholith. Metamorphism and crustal evolution of the western United States. , Rubey Volume
863 VII, p. 286-306. Prentice-Hall, Englewood Cliffs, NJ.
864 Gastil, R.G. (1975) Plutonic zones of the Peninsular Ranges of southern California and northern Baja
865 California. Geology, 3, 361-363.

Gelman, S.E., Deering, C.D., Bachmann, O., Huber, C., and Guiterrez, F.J. (2014) Identifying the crystal graveyards remaining after large silicic eruptions. Earth and Planetary Science Letters, 403, 299-306.

Gelman, S.E., Gutierrez, F.J., and Bachmann, O. (2013) On the longevity of large upper crustal silicic magma reservoirs. Geology, 41, 759-762.

Glazner, A.F., Coleman, D.R., and Bartley, J.M. (2008) The tenuous connection between high-silica rhyolites and granodiorite plutons. Geology, 36, 183-186.

Greene, A.R., DeBari, S.M., Kelemen, P.B., Blusztajn, J., and Clift, P.D. (2006) A detailed geochemical study of island arc crust: the Talkeetna arc section south-central Alaska. Journal of Petrology, 47, 1051-1093.

Gualda, G.A.R., Ghiorso, M.S., Lemons, R.V., and Carley, T.L. (2012) Rhyolite-Melts: a modified calibration of MELTS optimized for silica-rich, fluid-bearing magmatic systems. Journal of Petrology, 53, 875-890.

Hacker, B., Mehl, L., Kelemen, P., Rioux, M., Behn, M., and Luffi, P. (2008) Reconstruction of the Talkeetna intraoceanic arc of Alaska through thermobarometry. Journal of Geophysical Research, 113.

Hildreth, W. (1979) The Bishop Tuff: evidence for the origin of compositional zonation in silicic magma chambers. Geological Society of American Special Paper, 180, 43-75.

Hildreth, W., and Moorbath, S. (1988) Crustal contributions to arc magmatism in the Andes of central Chile. Contributions to Mineral Petrology, 98, 455-489.

Hildreth, W., and Wilson, C.J.N. (2007) Compositional zoning of the Bishop Tuff. Journal of Petrology, 48, 951-999.

Holloway, J.R., and Burnham, C.W. (1972) Melting relations of basalt with equilibrium water pressure less than total pressure. J. Petrology, 13, 1-29.

Huang, W.-L., and Wyllie, P.J. (1986) Phase relationships of gabbro-tonalite-granite-water at 15 kbar with applications to differentiatoin and anatexis. American Mineralogist, 71, 301-316.

Hui, H., and Zhang, Y. (2007) Toward a general viscosity equation for natural anhydrous and hydrous silicate melts. Geochimica et Cosmochimica Acta, 71, 403-416.

Hutchinson, R.M. (1956) Structure and petrology of Enchanted Rock Batholith, Llano and Gillespie counties, Texas. Geological Society of America Bulletin, 67, 763-806.

Jackson, M.D., Cheadle, M.J., and Atherton, M.P. (2003) Quantitative modeling of granitic melt generation and segregation in the continental crust. Journal of Geophysical Research, 108, doi:10.1029/2001J001050.

Jagoutz, O., and Schmidt, M.W. (2012) The formation and bulk composition of modern juvenile continental crust: the Kohistan arc. Chemical Geology, 298-299, 79-96.

Jagoutz, O.E. (2010) Construction of the granitoid crust of an island arc. Part II: a quantitative petrogenetic model. Contributions to Mineral Petrology, 160, 359-381.

Jahns, R.H., and Burnham, C.W. (1969) Experimental studies of pegmatite genesis: I. A model for the derivation and crystallization of granitic pegmatites. Economic Geology, 64, 843-864.

Kawamoto, T. (1996) Experimental constraints on differentiation and H_2O abundance of calc-alkaline magmas. Earth and Planetary Science Letters, 144, 577-589.

Kistler, R.W., Wooden, J.L., and Morton, D.M. (2003) Isotopes and ages in the northern Peninsular Ranges batholith, southern California. United States Geological Survey Open-File Report, 03-489, 45.

Kozeny, J. (1927) Uber kapillare leitung des wassers im boden. Sitzungsber, Akademie der Wissenschaften(136).

912 Lange, R.A., Cashman, K.V., and Navrotsky, A. (1994) Direct measurements of latent heat during
913 crystallization and melting of a ugandite and an olivine basalt. Contributions to Mineral
914 Petrology, 118, 169-181.
915 Langmuir, C.H. (1989) Geochemical consequences of in situ crystallization. Nature, 340, 199-205.
916 Lee, C.-T.A., and Bachmann, O. (2014) How important is the role of crystal fractionation in making
917 intermediate magmas? Insights from Zr and P systematics. Earth and Planetary Science Letters,
918 393, 266-274.
919 Lee, C.-T.A., Cheng, X., and Horodyskyj, U. (2006) The development and refinement of continental arcs
920 by primary basaltic magmatism, garnet pyroxenite accumulation, basaltic recharge and
921 delamination: insights from the Sierra Nevada, California. Contributions to Mineral Petrology,
922 151, 222-242.
923 Lee, C.-T.A., Lee, T.-C., and Wu, C.-T. (2013) Modeling the compositional evolution of recharging,
924 evacuating, and fractionating (REFC) magma chambers: implications for differentiation of arc
925 magmas. Geochimica et Cosmochimica Acta.
926 Lee, C.-T.A., Luffi, P., Chin, E.J., Bouchet, R., Dasgupta, R., Morton, D.M., Le Roux, V., Yin, Q.-Z., and Jin,
927 D. (2012) Copper systematics in arc magmas and implications for crust-mantle differentiation.
928 Science, 336(64), 64-68.
929 Lee, C.-T.A., and Morton, D.M. (2015) High silica granites: terminal porosity and crystal settling. Earth
930 and Planetary Science Letters, 409, 23-31.
931 Lee, C.-T.A., Morton, D.M., Kistler, R.W., and Baird, A.K. (2007) Petrology and tectonics of Phanerozoic
932 continent formation: from island arcs to accretion and continental arc magmatism. Earth and
933 Planetary Science Letters, 263, 370-387.
934 Lee, C.-T.A., Oka, M., Luffi, P., and Agranier, A. (2009) Internal distribution of Li and B in serpentinites
935 from the Feather River Ophiolite, California based on laser ablation inductively coupled plasma
936 mass spectrometry. Geochemistry, Geophysics, Geosystems, 9, doi:10.1029/2008GC002078.
937 Leighton, D., and Acrivos, A. (1987) measurement of shear-induced self-diffusion in concentrated
938 suspensions of spheres. Journal of Fluid Mechanics, 177, 109-131.
939 Lejeune, A.M., and Richet, P. (1995) Rheology of crystal-bearing silicate melts: an experimental study at
940 high viscosities. J. Geophys. Res., 100, 4215-4229.
941 Liao, K., Morton, D.M., and Lee, C.-T.A. (2013) Geochemical diagnostics of metasedimentary dark
942 enclaves: a case study from the Peninsular Ranges Batholith, southern California. International
943 Geology Review, 55, 1049-1072.
944 Lipman, P.W. (2007) Incremental assembly and prolonged consolidatio nof Cordilleran magma
945 chambers: evidence from the southern Rocky Mountain volcanic field. Geosphere, 3, 42.
946 Lundstrom, C. (2009) Hypothesis for the origin of convergent margin granitoids and Earth's continental
947 crust by thermal migration zone refining. Geochimica et Cosmochimica Acta, 73, 5709-5729.
948 Mader, H.M., Llewellin, E.W., and Mueller, S.P. (2013) The rheology of two phase magmas: a review and
949 analysis. Journal of Volcanology and Geothermal Research, 257, 135-158.
950 Marsh, B.D. (1981) On the crystallinity, probability of occurrence, and rheology of lava and magma.
951 Contributions to Mineralogy and Petrology, 78, 85-98.
952 McBirney, A.R. (1980) Mixing and unmixing of magmas. Journal of Volcanology and Geothermal
953 Research, 7, 357-371.
954 -. (1995) Mechanisms of differentiation in the Skaergaard intrusion. Journal of the Geological Society
955 London, 152, 421-435.
956 McKenzie, D. (1984) The generation and compaction of partially molten rock. Journal of Petrology, 25(3),
957 713-765.
958 -. (1987) The compaction of igneous and sedimentary rocks. Journal of the Geological Society London,
959 144, 299-307.

960 Miller, C.F., McDowell, S.M., and Mapes, R.W. (2003) Hot and cold granites? Implications of zircon
961 saturation temperatures and preservation of inheritance. Geology, 31, 529-532.
962 Mooney, M. (1951) The viscosity of a concentrated suspension of spherical particles. Journal of Colloid
963 Science, 6, 162-170.
964 Morton, D.M., Miller, F.K., Kistler, R.W., Premo, W.R., Lee, C.-T.A., Langenheim, V.E., Wooden, J.L., Snee,
965 L.W., Clausen, B.L., and Cossette, P. (2014) Framework and petrogenesis of the northern
966 Peninsular Ranges batholith, southern California. Geological Society of American Memoirs, 211,
967 61-143.
968 Noyes, H.J., Wones, D.R., and Frey, F.A. (1983) A tale of two plutons: petrographic and mineralogic
969 constraints on the petrogenesis of the Red Lake and Eagle Peak plutons, central Sierra Nevada,
970 California. Journal of Geology, 91, 353-379.
971 Pamukcu, A.S., Carley, T.L., Gulada, G.A.R., Miller, C.F., and Ferguson, C.A. (2013) The evolution of the
972 Peach Spring girant magma body: evidence from accessory mineral textures and compositions,
973 bulk pumice and glass geochemistry, and Rhyolite-MELTS modeling. Journal of Petrology, 54,
974 1109-1148.
975 Paterson, S.R., Vernon, R.H., and Tobisch, O.T. (1989) A review of criteria for the identification of
976 magmatic and tectonic foliations in granitoids. Journal of Structural Geology, 11, 349-363.
977 Patino Douce, A.E., and Johnston, A.D. (1991) Phase equilibria and melt productivity in the pelitic
978 system: implications for the origin of peraluminous granitoids and aluminous granulites.
979 Contributions to Mineral Petrology, 107, 202-218.
980 Philpotts, A.R. (1976) Silicate liquid immiscibility: its probable extent and petrogenetic significance.
981 American Journal of Science, 276, 1147-1177.
982 Pitcher, W.S. (1997) The nature and origin of granite. Chapman and Hall.
983 Plank, T., Kelley, K.A., Zimmer, M.M., Hauri, E.H., and Wallace, P.J. (2013) Why do mafic arc magmas
984 contain ~4 wt% water on average? Earth and Planetary Science Letters, 364, 168-179.
985 Putirka, K.D., Canchola, J., Rash, J., Smith, O., Torrez, G., Paterson, S.R., and Ducea, M.N. (2014) Pluton
986 assembly and the genesis of granitic magmas: insights from the GIC pluton in cross section.
987 Sierra Nevada Batholith, California. Am. Mineral., 99, 1284-1303.
988 Putirka, K.D., Perfit, M., Ryerson, F.J., and Jackson, M.G. (2007) Ambient and excess mantle
989 temperatures, olivine thermometry, and active vs. passive upwelling. Chemical Geology, 241,
990 177-206.
991 Rabinowicz, M., Genthon, P., Ceuleneer, G., and Hillairet, M. (2001) Compaction in a mantle mush with
992 high melt concentrations and the generation of magma chambers. Earth and Planetary Science
993 Letters, 188, 313-328.
994 Ratajeski, K., Sisson, T.W., and Glazner, A.F. (2005) Experimental and geochemical evidence for
995 derivation of the El Capitan Granite, California, by partial melting of hydrous gabbroic lower
996 crust. Contributions to Mineral Petrology, 149, 713-734.
997 Richardson, J.F., and Zaki, W.N. (1954) The sedimentation of a suspension of uniform spheres under
998 conditions of viscous flow. Chemical Engineering Science, 3, 65-73.
999 Roedder, E. (1951) Low-temperature liquid immiscibility in the system K_2O-FeO-Al_2O_3-SiO_2. American
1000 Mineralogist, 84, 1346-1353.
1001 Rosing, M.T., Bird, D.K., Sleep, N.H., Glassley, W., and Albarede, F. (2006) The rise of continents - an
1002 essay on the geologic consequences of photosynthesis. Palaeogeography, Palaeoclimatology,
1003 Palaeoecology, 232, 99-113.
1004 Ross, M.E. (1986) Flow differentiation, phenocryst alignment, and compositional trends within a dolerite
1005 dike at Rockport, Massachusetts. Geological Society of America Bulletin, 97, 232-240.
1006 Rutter, M.J., and Wyllie, P.J. (1988) Melting of vapour-absent tonalite at 10 kbar to simulate
1007 dehydration-melting in the deep crust. Nature, 331, 159-160.

Saar, M.O., Manga, M., Cashman, K.V., and Fremouw, S. (2001) Numerical models of the onset of yield strength in crystal-melt suspensions. Earth and Planetary Science Letters, 187, 367-379.

Scaillet, B., Holtz, F., and Pichavant, M. (1997) Rheological properties of granitic magmas in their crystallization range. In J.L. Bouchez, D.H.W. Hutton, and W.E. Stephens, Eds. Granite: from segregation of melt to emplacement fabrics, p. 11-29. Kluwer, Dordrecht, Netherlands.

Scott, T., and Kohlstedt, D.L. (2006) The effect of large melt fraction on deformation behavior of peridotite. Earth and Planetary Science Letters, 246, 177-187.

Snabre, P., and Pouligny, B. (2008) Size segregation in a fluid-like or gel-like suspension settling under gravity or in a centrifuge. Langmuir, 24, 13338-13347.

Taylor, S.R., and McLennan, S.M. (1985) The continental crust: its composition and evolution. Blackwell, Oxford.

Todd, V.R., Erskine, B.G., and Morton, D.M. (1988) Metamorphic and tectonic evolution of the Penisular Ranges batholith. In W.G. Ernst, Ed. Metamorphism and crustal evolution of the western United States, Rubey Volume VII, p. 894-937. Prentice-Hall, Englewood Cliffs, NJ.

Turi, B., and Taylor, H.P., Jr. (1971) An oxygen and hydrogen isotope study of a granodiorite pluton from the southern California batholith. Geochimica et Cosmochimica Acta, 35, 383-406.

Tuttle, O.F., and Bowen, N.L. (1958) Origin of granite in the light of experimental studies in the system $NaAlSi_3O_8$-$KAlSi_3O_8$-SiO_2-H_2O. Geological Society of American Memoirs, 74, 1-146.

Van Tongeren, J.A., and Mathez, E.A. (2012) Large-scale liquid immiscibility at the top of the Bushveld Complex. Geology, 40, 491-494.

Vernon, R.H. (1986) K-feldspar megacrysts in granites - phenocrysts, not porphyroblasts. Earth-Science Reviews, 23, 1-63.

Vielzeuf, D., and Schmidt, M.W. (2001) Melting relations in hydrous systems revisited: application to metapelites, metagreywackes and metabasalts. Contributions to Mineral Petrology, 141, 251-267.

Wade, J.A., Plank, T., Stern, R.J., Tollstrup, D.L., Gill, J.B., O'Leary, J.C., Eiler, J.M., Moore, R.B., Woodhead, J.D., Trusdell, F., Fischer, T.P., and Hilton, D.R. (2005) The may 2003 eruption of Anatahan volcano, Mariana Islands: geochemical evolution of a silicic island-arc volcano. Journal of Volcanology and Geothermal Research, 146, 139-170.

Wark, D.A., and Watson, E.B. (2006) TitaniQ: a titanium-in-quartz geothermometer. Contrib. Mineral. Petrol., 152, 743-754.

Warren, P.H., Taylor, G.J., Keil, K., Shirley, D.N., and Wasson, J.T. (1983) Petrology and chemistry of two "large" granite clasts from the moon. Earth and Planetary Science Letters, 64, 175-185.

Watson, E.B., and Harrison, T.M. (1983) Zircon saturation revisited: temperature and composition effects in a variety of crustal magma types. Earth and Planetary Science Letters, 64, 295-304.

-. (2005) Zircon thermometer reveals minimum melting conditions on earliest Earth. Science, 841-844.

Whittington, A.G., Hofmeister, A.M., and Nabelek, P.I. (2009) Temperature-dependent thermal diffusivity of Earth's crust and implications for magmatism. Nature, 458, 319-321.

Figure 1

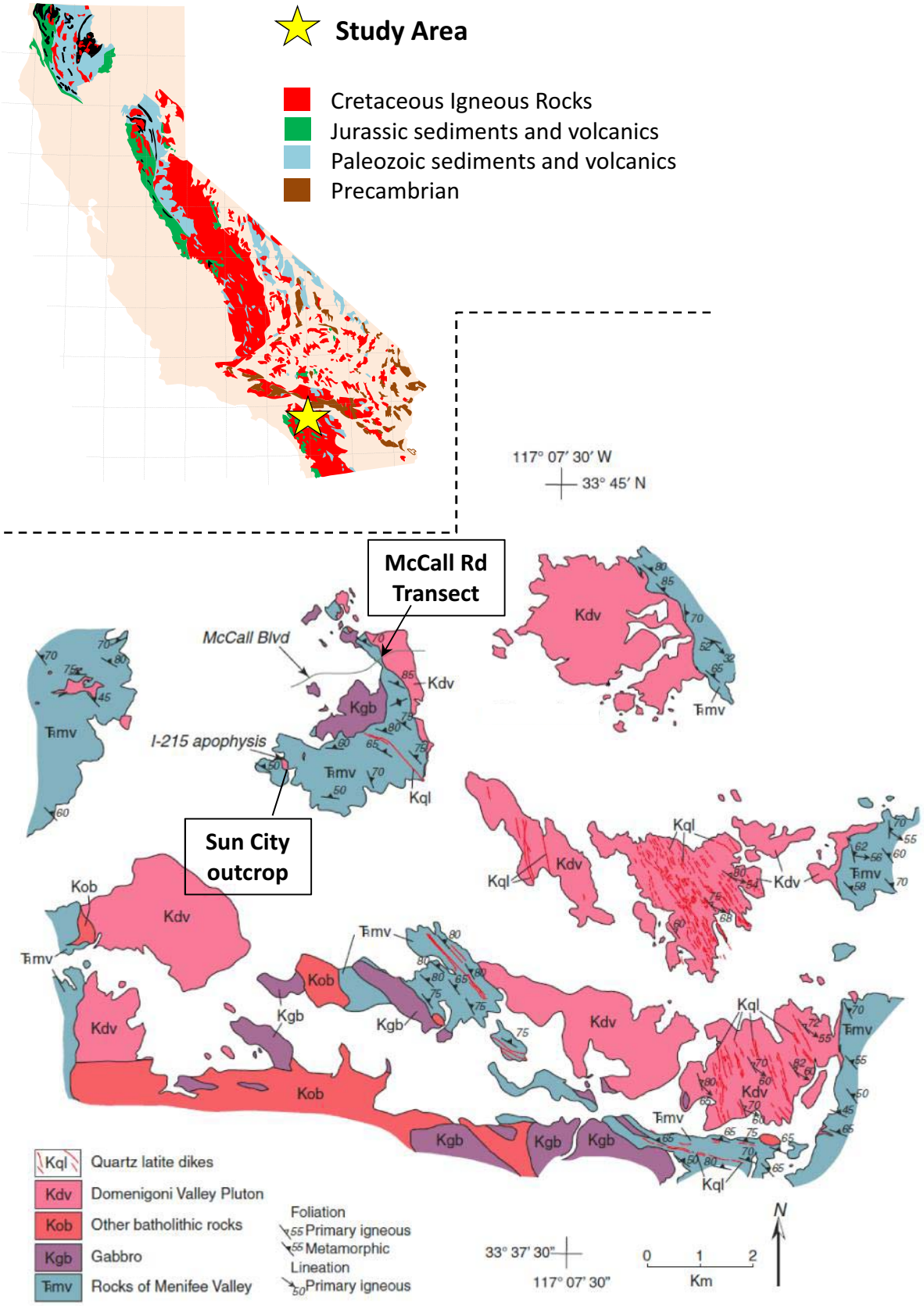
Study Area
Cretaceous Igneous Rocks
Jurassic sediments and volcanics
Paleozoic sediments and volcanics
Precambrian
117° 07′ 30′ W
33° 45′ N
McCall Rd Transect
McCall Blvd
I-215 apophysis
Sun City outcrop
Kdv
Kgb
Kob
Kql
Tmv
Quartz latite dikes
Domenigoni Valley Pluton
Other batholithic rocks
Gabbro
Rocks of Menifee Valley
Foliation
Primary igneous
Metamorphic
Lineation
Primary igneous
33° 37′ 30″
117° 07′ 30″
0 1 2
Km
N

This is a preprint, the final version is subject to change, of the American Mineralogist (MSA)
Cite as Authors (Year) Title. American Mineralogist, in press.
(DOI will not work until issue is live.) DOI: http://dx.doi.org/10.2138/am-2015-5121

Figure 2

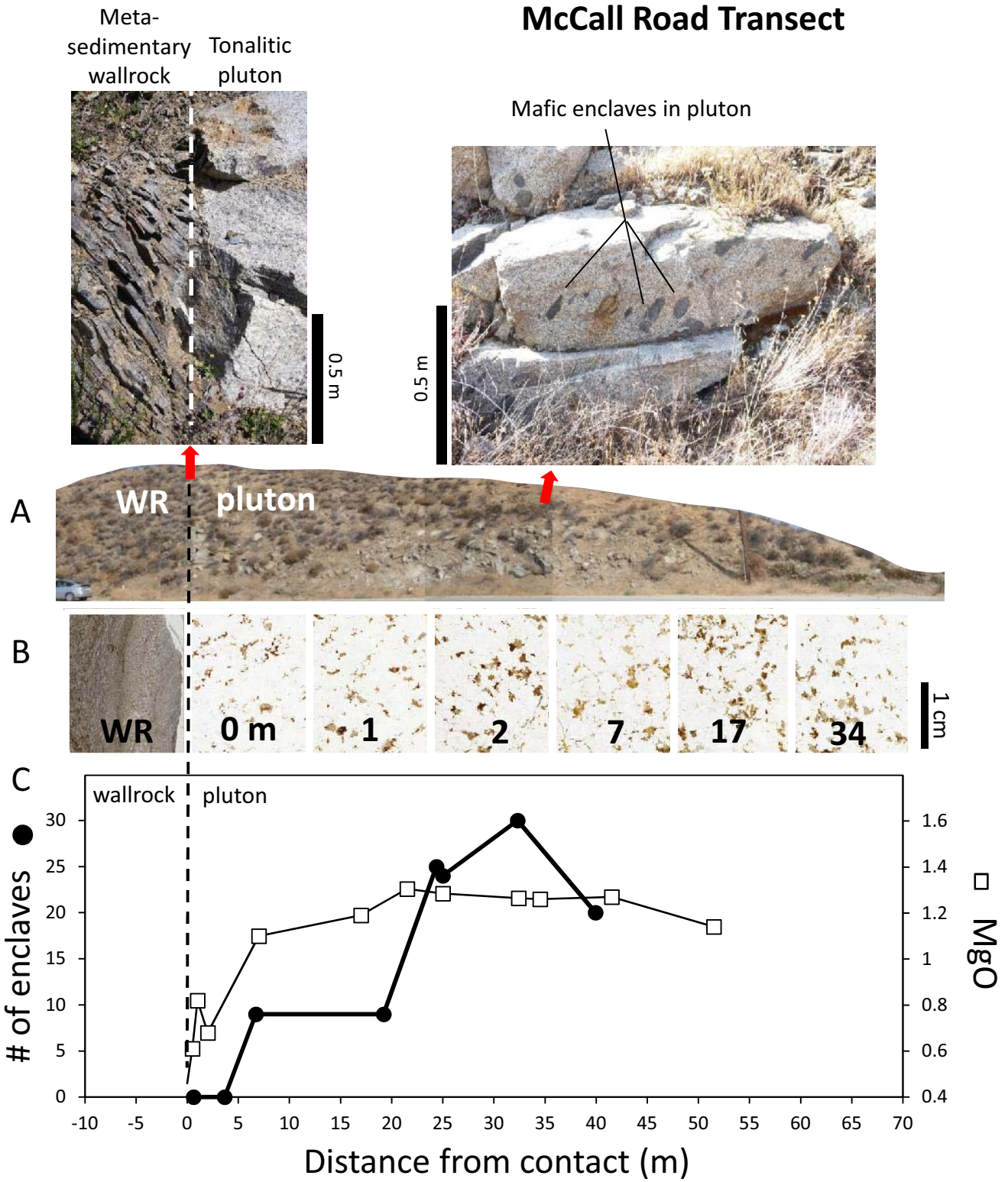

This is a preprint, the final version is subject to change, of the American Mineralogist (MSA)
Cite as Authors (Year) Title. American Mineralogist, in press.
(DOI will not work until issue is live.) DOI: http://dx.doi.org/10.2138/am-2015-5121

Figure 3

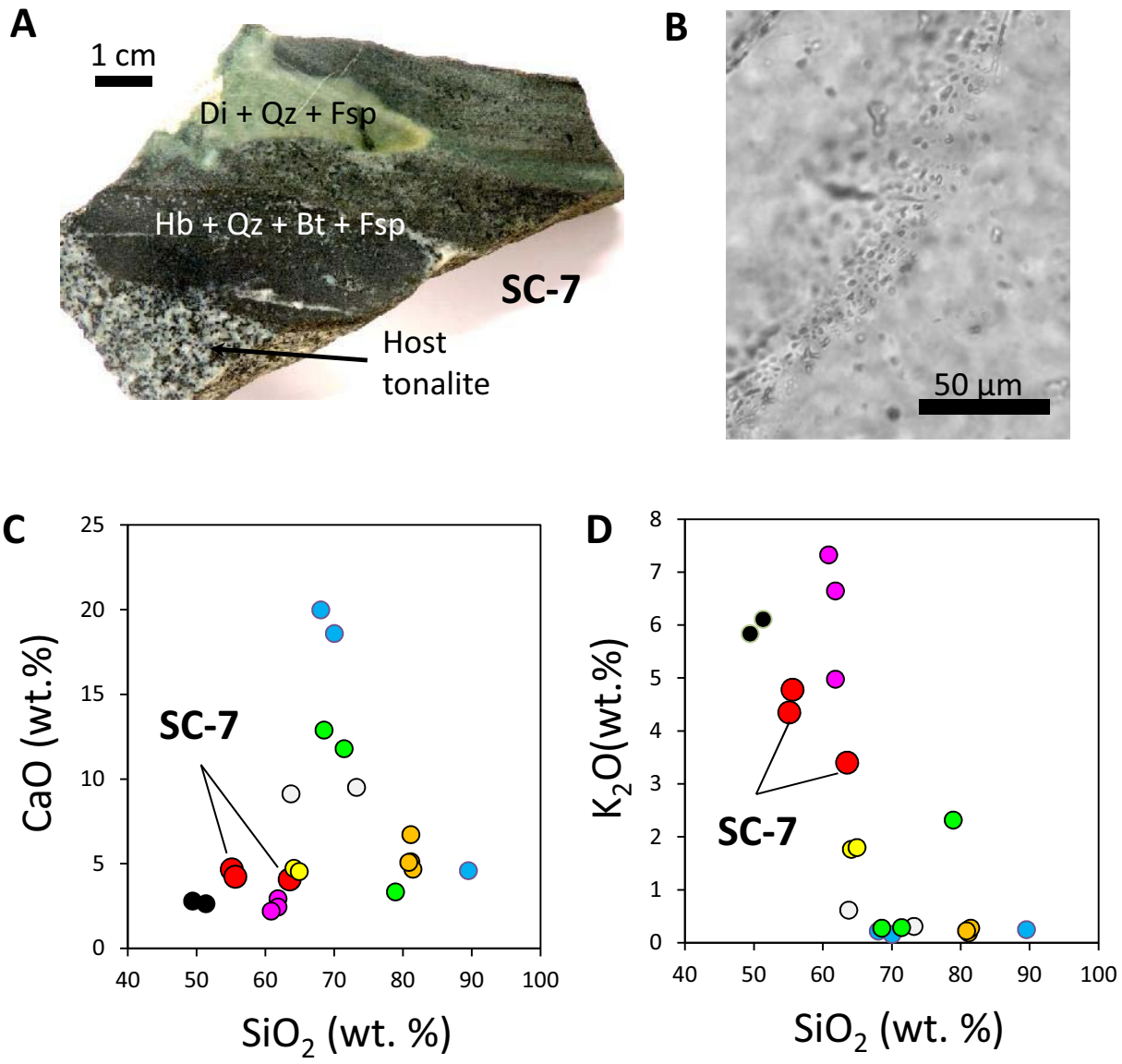

Figure 4

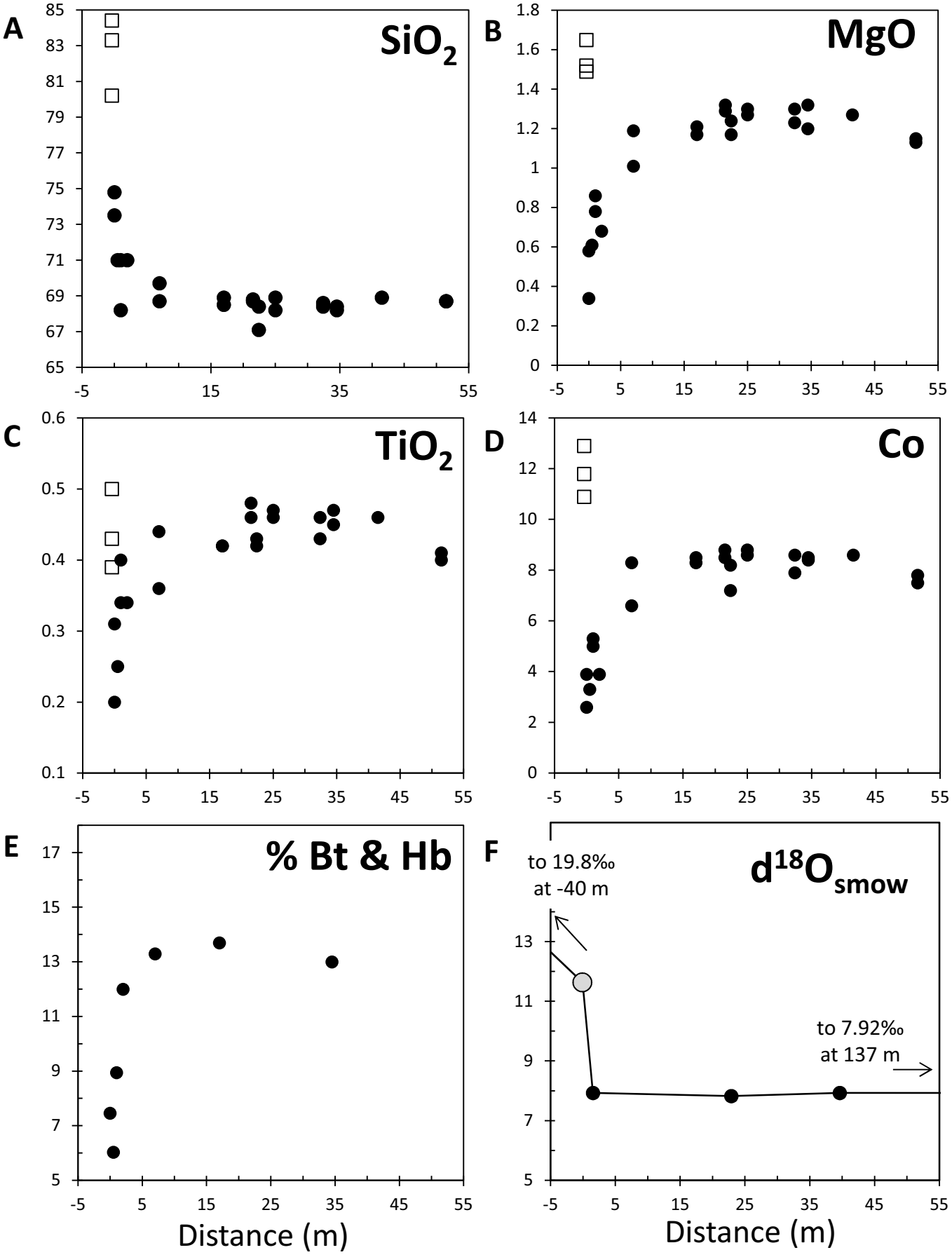
A
SiO2
B
MgO
C
TiO2
D
Co
E
% Bt & Hb
Distance (m)
F
d18Osmow
to 19.8‰
at -40 m
to 7.92‰
at 137 m
Distance (m)

This is a preprint, the final version is subject to change, of the American Mineralogist (MSA)
Cite as Authors (Year) Title. American Mineralogist, in press.
(DOI will not work until issue is live.) DOI: http://dx.doi.org/10.2138/am-2015-5121

Figure 5

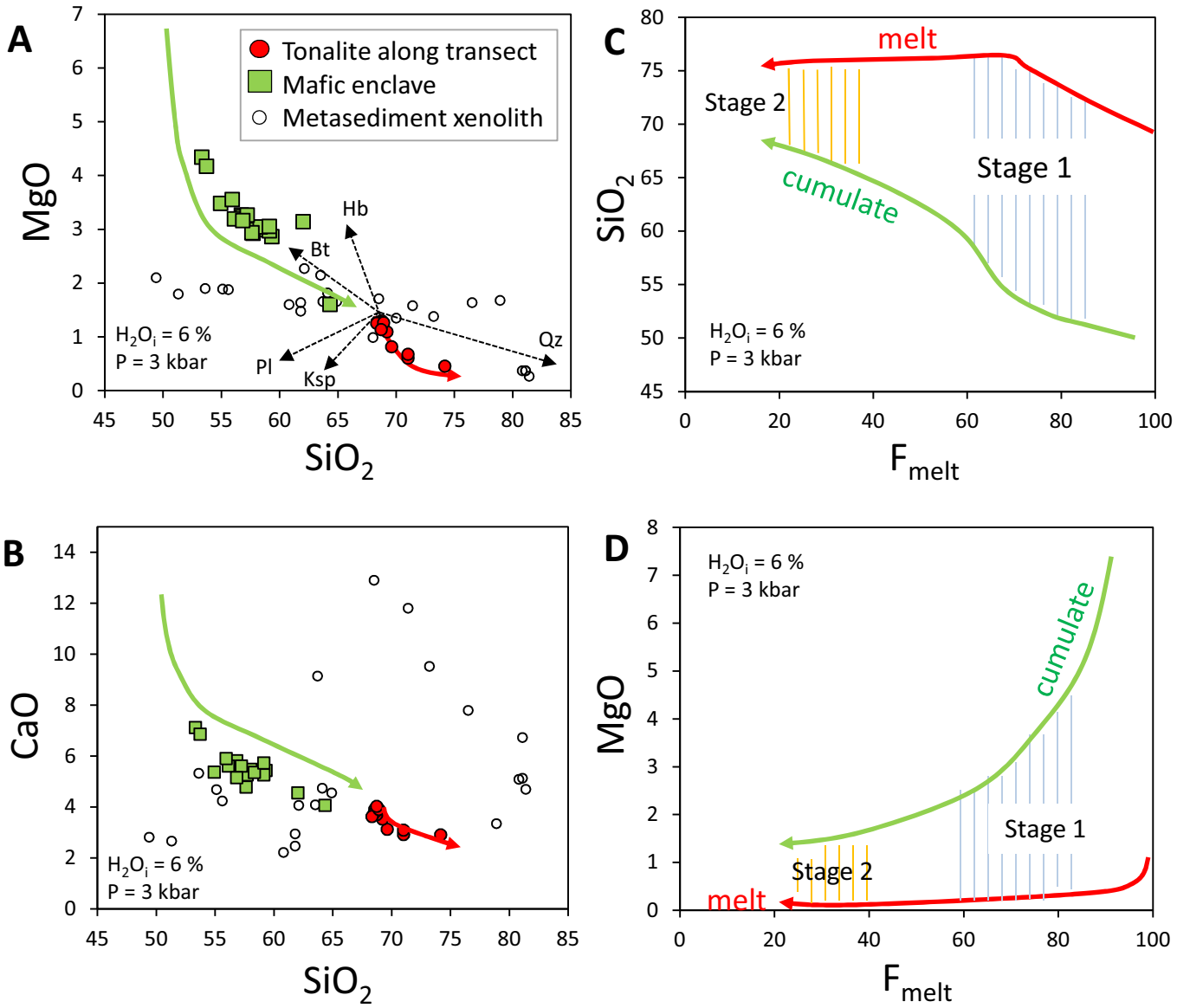

Figure 6

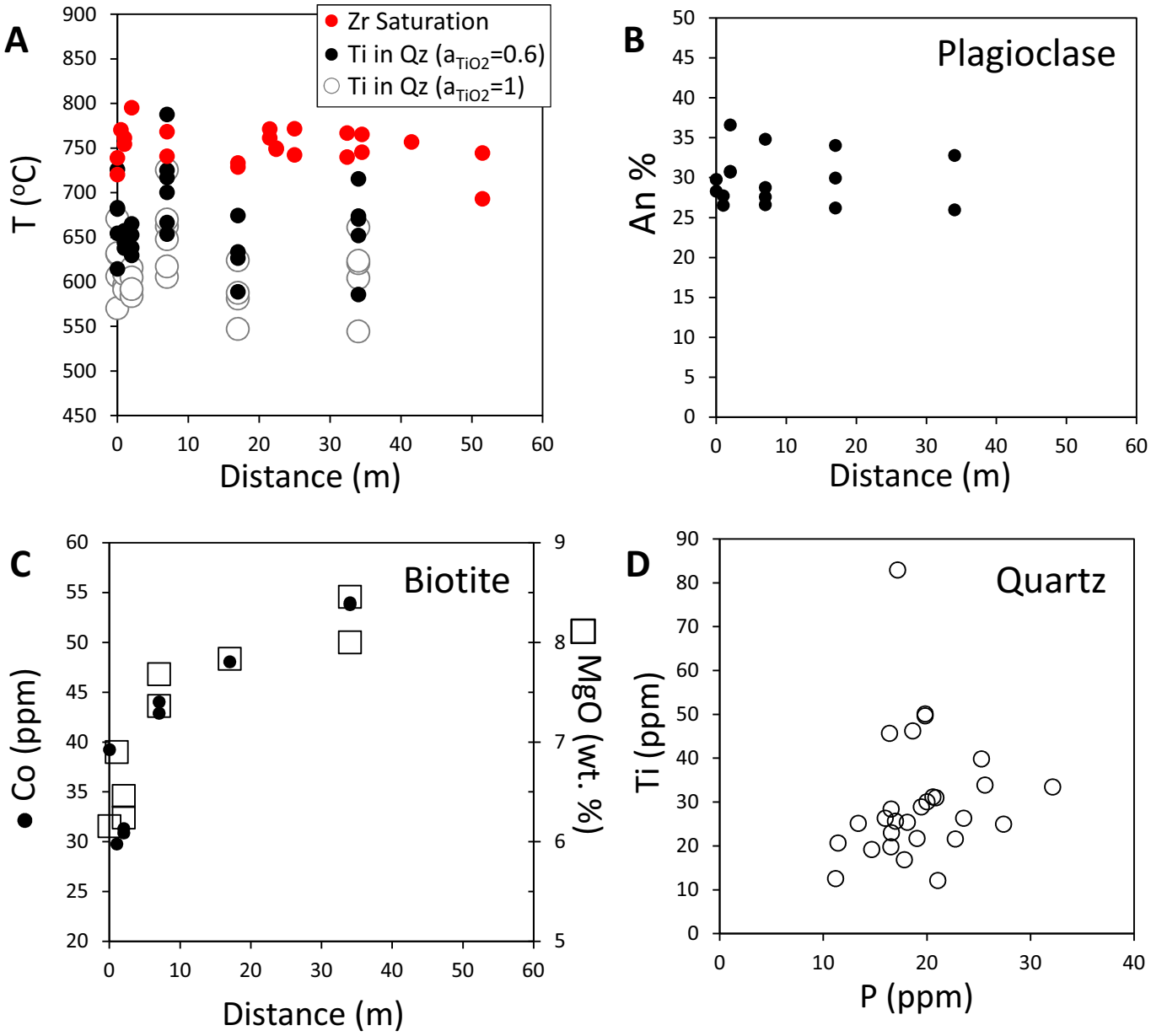
A
Zr Saturation
Ti in Qz (a_{TiO2}=0.6)
Ti in Qz (a_{TiO2}=1)
T (°C)
Distance (m)
B
Plagioclase
An %
Distance (m)
C
Biotite
Co (ppm)
MgO (wt. %)
Distance (m)
D
Quartz
Ti (ppm)
P (ppm)

This is a preprint, the final version is subject to change, of the American Mineralogist (MSA)
Cite as Authors (Year) Title. American Mineralogist, in press.
(DOI will not work until issue is live.) DOI: http://dx.doi.org/10.2138/am-2015-5121

Figure 7

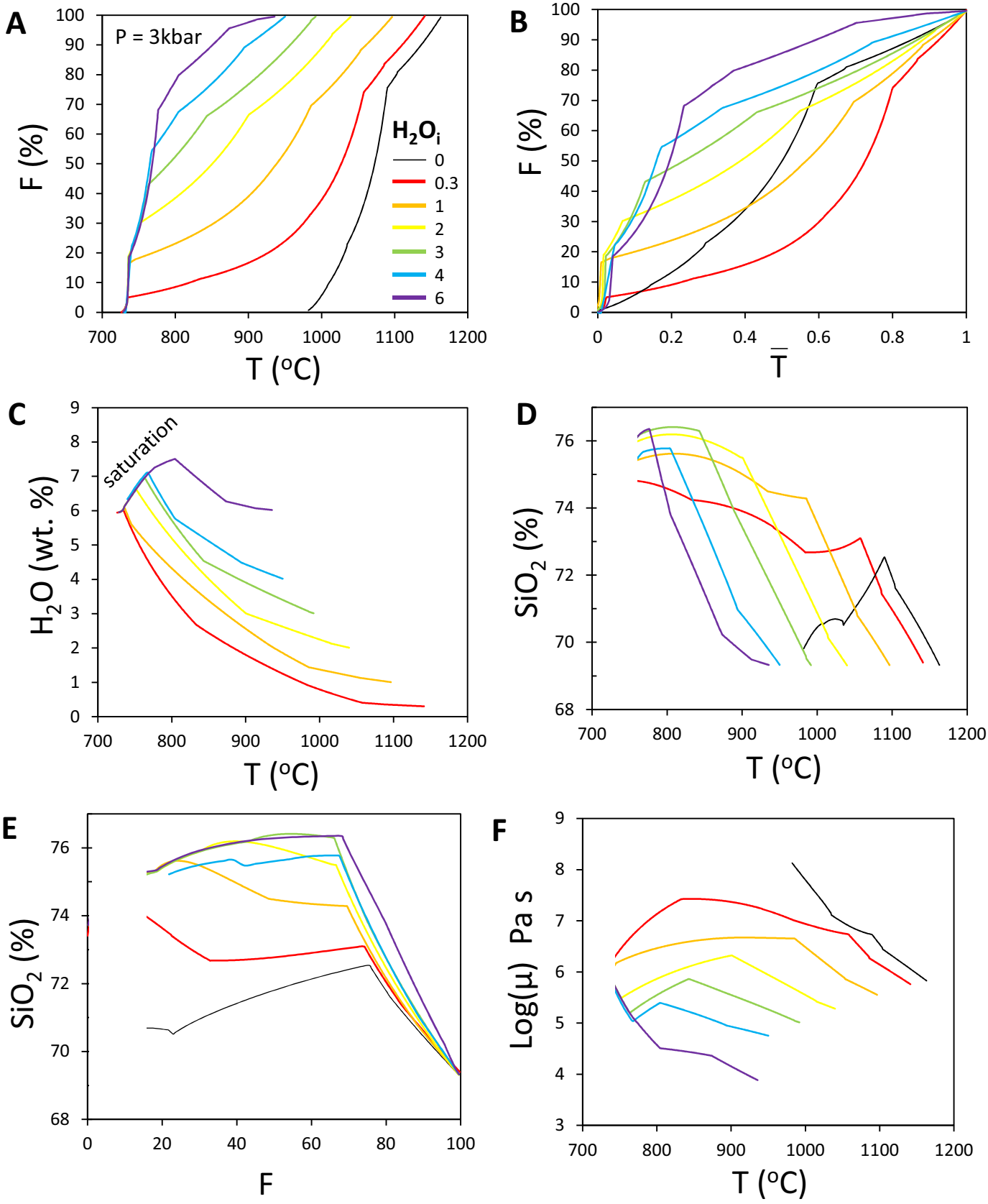

This is a preprint, the final version is subject to change, of the American Mineralogist (MSA)
Cite as Authors (Year) Title. American Mineralogist, in press.
(DOI will not work until issue is live.) DOI: http://dx.doi.org/10.2138/am-2015-5121

Figure 8

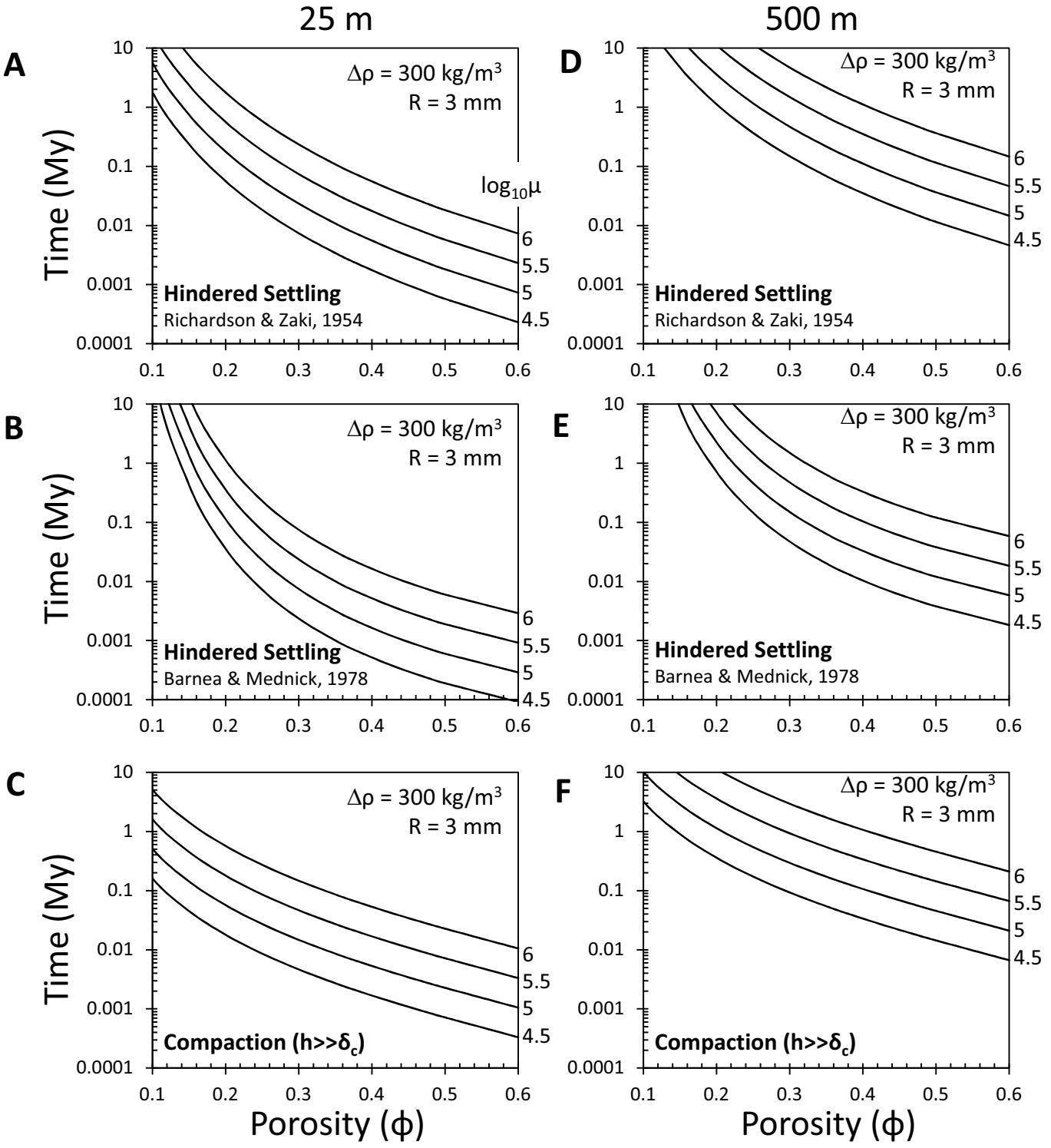

This is a preprint, the final version is subject to change, of the American Mineralogist (MSA)
Cite as Authors (Year) Title. American Mineralogist, in press.
(DOI will not work until issue is live.) DOI: http://dx.doi.org/10.2138/am-2015-5121

Figure 9

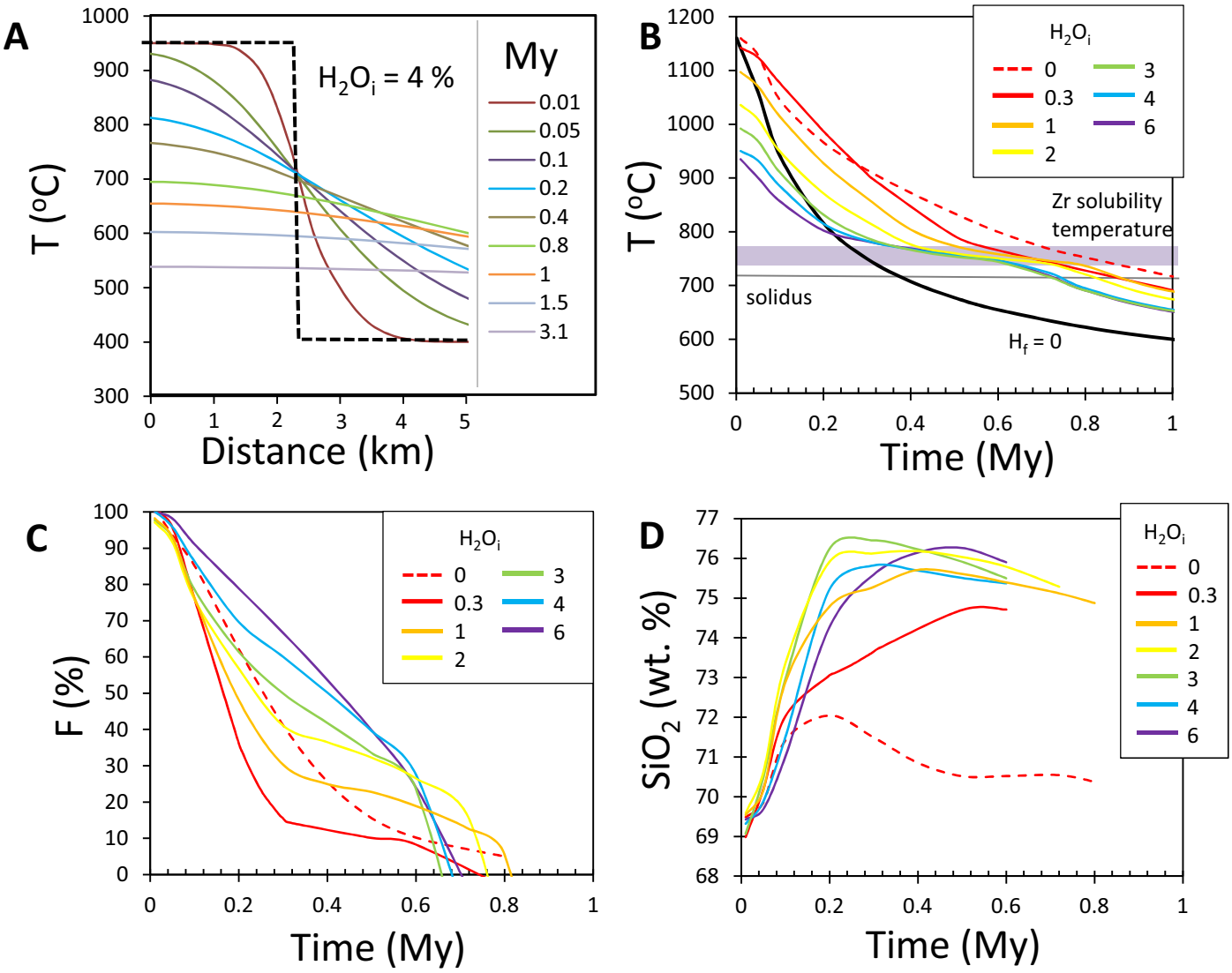

Figure 10

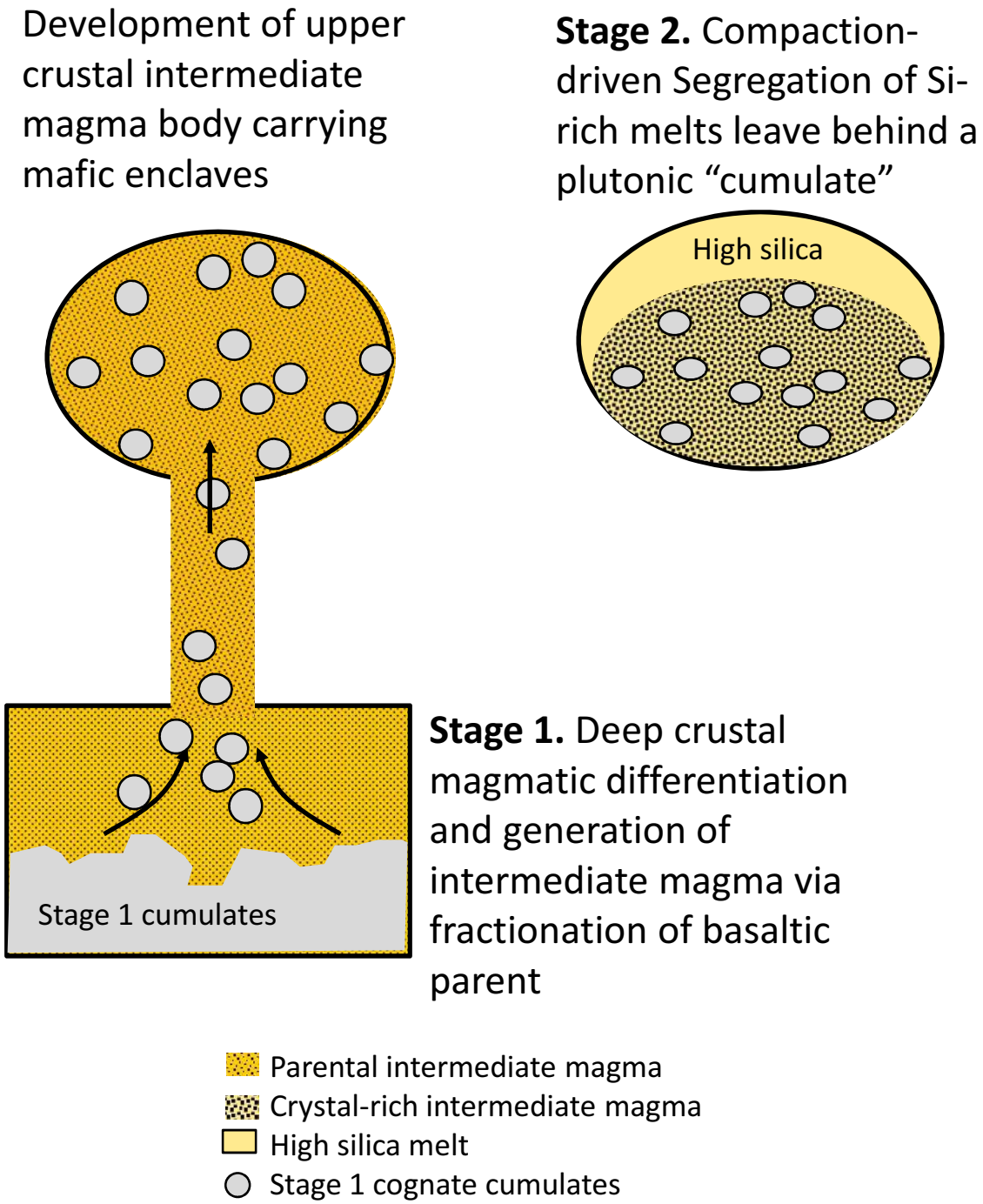
Development of upper crustal intermediate magma body carrying mafic enclaves
Stage 2. Compaction-driven Segregation of Si-rich melts leave behind a plutonic "cumulate"
High silica
Stage 1 cumulates
Stage 1. Deep crustal magmatic differentiation and generation of intermediate magma via fractionation of basaltic parent
Parental intermediate magma
Crystal-rich intermediate magma
High silica melt
Stage 1 cognate cumulates